2019-01-01

Phase Diagram of Nuclear Matter

Adrian Gaytan Terrazas
University of Texas at El Paso

PHASE DIAGRAM OF NUCLEAR MATTER

ADRIÁN GAYTÁN TERRAZAS

Master's Program in Physics

APPROVED:

Jorge Alberto López, Ph.D, Chair.

Ramon Ravelo, Ph.D.

Rajendra Zope, Ph.D.

Luis Valdez, Ph. D.

Stephen Crites, Ph.D.
Dean of the Graduate School

Dedicated to my

MOTHER, FATHER and SISTER

with love

PHASE DIAGRAM OF NUCLEAR MATTER

by

ADRIÁN GAYTÁN TERRAZAS

THESIS

Presented to the Faculty of the Graduate School of

The University of Texas at El Paso

in Partial Fulfillment

of the Requirements

for the Degree of

MASTER OF SCIENCE

Department of Physics

THE UNIVERSITY OF TEXAS AT EL PASO

December 2019

Acknowledgements

I would like to express my gratitude to my family; mi mother, my father, my sister, and my grandparents, that always were present giving me all kinds of support during this process. Without them this couldn't be possible.

As well I would like to thank my advisor, who constantly guided me with patience and dedication since the first day we started working.

NOTE: This thesis was submitted to my Supervising Committee on the November 31, 2019.

Abstract

Nowadays it is well known that nuclear matter has a liquid and a gas phase, as well as a coexistence of phases region. Symmetric nuclear matter (same number of protons and neutrons) exhibit phase transitions from the gas phase to a liquid-gas mixture. A useful tool to represent such phases and transitions is through diagrams that show the necessary conditions of density and temperature to be in either of the phases. Now the question is, what if we extend the traditional phase diagram for symmetric matter to the asymmetric cases (different number of protons and neutrons)?

This study uses classical molecular dynamics to simulate infinite nuclear matter and study the effect of isospin asymmetry on bulk properties such as energy per nucleon, pressure, density, as well as the coexistence of phases region in nuclear matter. The simulations are performed on systems embedded in periodic boundary conditions with densities and temperatures in the ranges $\rho = 0.01$ to $0.2 fm^{-3}$ and $T = 1$ to $15 MeV$, and with isospin content of $X = Z/A = 0.3$, 0.35, 0.4, 0.45, and 0.5, where Z refers to the number of protons and A the total number of nucleons.

The results indicate that the main effect of isospin asymmetry is found to be the disappearance of the liquid-gas phase transition when $X = Z/A = 0.13$.

Particularly in this study we obtain the phase diagram of nuclear matter extending it from the traditional two-dimensional density-temperature plane to three-dimensional space of density, temperature, and isospin asymmetry. We identify the liquid-gas coexistence region by means of Maxwell constructions over pressure-volume isotherms.

Table of Contents

List of Tables

List of Figures

Chapter 1

Introduction

Many research facilities have been performing experiments using neutron-rich nuclei to extend our knowledge of nuclear forces. These reactions between radioactive nuclei can help us understand properties of isospin asymmetric nuclear matter, needed in several areas of physics [1].

The importance of asymmetric nuclear matter, and how it affects the nuclear forces, was noticed by Weizsäcker in 1935 [2] when he introduced an asymmetry term in a parametrization of the nuclear binding energy in favor of the condition $A = 2Z$, where Z refers to the number of protons and A to the total number of nucleons. In the next decades this investigation was extended to study the isospin dependence of a generalized density-dependent asymmetry term [3], as well as other nuclear properties [4]. A limitation of the asymmetry term of Bethe-Weizsäcker parametrization is that when $N = Z$ (same number of protons and neutrons), it does not show appropriate results in nuclei of $A > 40$. The problem is that for this type of nuclei we need the presence of a higher quantity of neutrons to compensate the long-range Coulomb repulsion.

On the other hand, there have been several attempts to extend the liquid-drop formula into the isospin asymmetric cases; the strategy was to represent the nuclear energy $E(\rho, \alpha)$ in terms of $\alpha = (N - Z)/A$ about the isospin symmetric point $\alpha = 0$: $E(\rho, \alpha) = E(\rho, \alpha = 0) + E_{Sym}(\rho)\alpha^2 + O(\alpha^4)$ [3]. In the same way these expressions can be used to obtain a density-dependent symmetry energy through $E_{Sym}(\rho) = (1/2!)(\partial^2 E/\partial\alpha^2)$, but producing modest results in comparison to experimental data [3]

At this point, with the limitations of the parametrizations, one may think that a better option to follow would be through the use of microscopic theories to develop an equation of

state dependent of density, temperature and isospin, unfortunately, we would have to deal with many body theories, which is far of being perfect, and only produced modest results at low temperatures. For example, studies obtained with Hartree-Fock approximations [10, 11, 12, 13, 14, 15, 16], for studies with relativistic and non-relativistic mean-field models [17, 18, 19, 20, 21, 22, 23, 24], and for non-zero temperature studies [1].

Nevertheless, a way that one can follow to avoid these technical difficulties is through numerical methods to construct systems where we can extract desired properties of nuclear matter. One of the most used methods is known as Classical Molecular Dynamics (CMD); this is not a new method, actually, it has been used for decades to study nuclear reactions [25, 26, 27, 28], and more recently to get properties of infinite systems as found in neutron star crusts [29, 30, 31, 32, 33, 34, 35, 36], as well as on the isospin dependence of nuclear matter properties [4].

In particular, CMD studies [33, 34, 35, 37, 36] have investigated phases in low temperature nuclear matter, as they exist in neutron star crusts, and the effect of isospin asymmetry on bulk properties such as energy per nucleon, pressure, saturation density, compressibility, and symmetry energy [4]. The results of these studies indicate that symmetric and asymmetric nuclear matter show liquid and gaseous phases and transitions between them, as well as the coexistence of phases regions that tend to be reduced because of the isospin content.

1.1 Objectives

In view of the need to see how the isospin content affects the properties, as well as the approximations to describe nuclear matter, the motivation of this study is the extension of the traditional two-dimensional phase diagram (which correspond to symmetric nuclear matter) to include the isospin content degree of freedom.

The phase diagram is usually represented in the two-dimensional density-temperature plane, but now it would span a volume in the $\rho - \alpha - T$ space. Here we use CMD to study infinite nuclear systems with varying density, temperature and isospin content to obtain pressure-density isotherms and, from them, extract the boundary of the liquid-gas phase coexistence region by means of Maxwell constructions for temperatures that go from $T = 1MeV$ to $15MeV$.

The structure of the thesis is as follows: Section II introduces the computational model used (CMD), all data obtained from the simulations will be presented on section III, followed on Section IV by showing a procedure which is vital for our study; Maxwell's construction, the desired Phase Diagrams in section V, and lastly, the conclusions of the study in section VI.

1.2 Metodology

To achieve our goals, we will construct systems of infinite nuclear matter with different isospin content and temperature T using numerical simulations on the interval of our interest.

From the simulations we are interested on getting the energy and pressure in terms of density from such systems, then, turn the obtained pressure vs density curves into pressure vs volume to use them on the Maxwell construction process.

With the density delimitations we will construct two-dimensional phase diagrams that includes al temperatures in our interval for each value of X. Finally, we combine the

individual diagrams on the three-dimensional diagram that includes the isospin degree of freedom.

Chapter 2

Computational Model

2.1 Classical Molecular Dynamics

There are several numerical methods to study many-body nuclear systems, CMD is just one of them. Another of the most used methods are known as semiclassical models (BUU, IBUU) and quantum molecular dynamics models (QMD, AMD, IQMD, etc. [39, 40, 41]). The problem with these methods is that they have a limitation, even when they predict accurately density fluctuations in heavy-ion reactions, they both fail to produce realistic clusters [38], which means they cannot be used to the study of phase transitions.

The advantage of using CMD instead semiclassical and quantum models is that this method does not have adjustable parameters such as wavepackets, mean fields, effective masses and cross sections [42]. What CMD does is consider the protons and neutrons as interacting particles through potentials with their classical equations of motion solved numerically. This means that a lot of systems can be described using this method, for example; cold nuclei, nuclear reactions, phase transitions and infinite systems as neutron star crust [29, 30, 31, 32, 33, 34, 35, 36].

The only disadvantage of using CMD is the lack of Pauli blocking, which does not allow us to get appropriate results at low energies. Fortunately, in hot systems ($T \geq 1$ MeV), the results do not get affected by this limitation [4].

2.2 Potential

Since CMD works with potentials, several of them have been used in the past [25, 26, 27, 28], but there is strong evidence that says that the main characteristics of the phases in nuclear matter are not affected wherever the potential we choose [37]. In our study we are going to use the Pandharipande potentials which were designed at the University of Illinois Urbana-Champaign to fit experimental nucleon-nucleon collisions of up to $600MeV$ to produce infinite systems with realistic binding energy, density, and compressibility comparable to experimental results. This potential describes the motion of nucleons by solving their classical equations of motion.

The Pandharipande potentials are [26]:

$$V_{np}(r) = V_r[exp(-\mu_r r)/r - exp(-\mu_r r_c)/r_c - V_a[exp(-\mu_a r)/r - exp(-\mu_a r_c)/r_c \qquad (2.1)$$

$$V_{NN}(r) = V_{nn}(r) = V_{pp}(r) = V_0[exp(-\mu_0 r)/r - exp(-\mu_0 r_c)/r_c \qquad (2.2)$$

where V_{np} is the potential between a neutron and a proton, and V_{NN} is the repulsive interaction between either nn or pp, and all the values of the parameters are given in table 2.1. The cutoff radius $r_c = 5.4\ fm$ (known as cutoff length; the distance after which you will neglect all the other particles, because you consider their influence on the present to be zero). Both potentials are set to zero when $r > r_c$.

The Yukawa parameters μ_r, μ_a and μ_0 were determined by Pandharipande to yield an equilibrium density of $\rho_0 = 0.16\ fm^{-3}$, a binding energy $E(\rho_0) = 16$ MeV/nucleon. Notice that, since the potential V_{NN} does not permit bound states between identical nucleons,

Table 2.1: Parameters of Pandharipande potentials

r_c	V_r	V_a	V_0	μ_r	μ_a	μ_0
$5.4fm$	3088.118	2666.647	373.118	1.7468	1.6000	1.500

pure neutron matter is unbound and, at a difference from potentials used by other models, the Pandharipande potentials have a hard core. A more complete description of the Pandharipande potentials can be found elsewhere [26].

The main advantage of the CMD model is the possibility of knowing the position and momentum of all particles at all times, which allow us to study the structure of the nuclear media from a microscopic point of view. Even more, CMD provides the time evolution of the particles, which is then used to study the resulting structures.

To simulate nuclear matter as an infinite medium, systems with thousands of nucleons were constructed using CMD under periodic boundary conditions. Cases symmetric in isospin (i.e. with $X = Z/A = 0.5$, 1000 protons and 1000 neutrons), and cases with asymmetric isospin (with $X = 0.3, 0.35, 0.4$ and 0.45) were constructed in cubical boxes with sizes adjusted to have densities between $0.01 fm^{-3}$ and $0.2 fm^{-3}$. Once the cubical box is filled with the appropriate amount of particles and density, the box with its particles is then replicated in the 26 cells surrounding the box to guarantee periodic boundaries.

Chapter 3

CMD Results

3.1 Classical Molecular Dynamics Set Up Description

For the study of infinite systems of nuclear matter, we used a CMD code fitted with the Pandharipande potentials [53]. With this model we simulated the evolution of 2000 nucleons inside a cubic cell with periodic boundary conditions. The isospin content had values of $X = Z/A = 0.3, 0.35, 0.4, 0.45$ and 0.5 (where Z is the number of protons and A the total number of nucleons), densities between $0.01 fm^{-3}$ and $0.2 fm^{-3}$, and temperatures that went from $T = 1$ to $15 MeV$. The nucleons were placed in random positions with a minimum interparticle distance of $0.01 fm$ and initial velocities according to the Maxwell-Boltzmann distribution at the desired temperature. Finally, the equations of motion were solved to simulate the evolution of the system.

Because this calculations take long times to be performed, a heat reservoir was added to the newtonian mechanics to speed up the process yielding the Nosé-Hoover equations of motion which were integrated by Størmer finite differences; although this method does not conserve energy (which is added or removed by the heat reservoir), it reaches thermal equilibrium faster than the usual formalism of newtonian mechanics plus an Andersen's thermostat [54].

Once that all the conditions are set up, we let the system evolve until it reaches equilibrium (determined by variations of $\Delta T < 0.1\%$), at this point we collect and store the pertinent data such as nucleon positions, momenta, energy per nucleon, pressure, temperature, and density. Now that we have our first data stored, we let the system evolve again to get data of the system in a different time that must be far enough from the first time, so

they are not related to each other. Finally, we repeat the process to form a Markov chain.

3.2 Average Energy and Pressure

From the simulations, we obtained values of average energy and pressure for each proportion X, temperature T, and density ρ. To get each point for the average energy we took values from the list of energies that the code gives us as result, those values needed to be far away enough in tome in order to not have relation between them. With these values we formed a Markov chain making sure that the percentage of error was less than 10% for each of such points. The tables that contain the average energy values will be shown at the end of the document in appendix A of energy tables, meanwhile, on figures 3.1, 3.2, 3.3, 3.4, and 3.5 we show such values corresponding to these energies for each of the proportions.

In the energy plots it is clear to see a characteristic "$\cup$" shape that is expected for this type of curves; this region contains information of the phases of the system.

Meanwhile, in the pressure curves 3.6, 3.7, 3.8, 3.9, and 3.10, we see a behavior where the slope of the curve is always positive $\partial p/\partial \rho > 0$. As well as for the energy, this pressure curves contain information about the phases, and they will be used later in other procedure in this thesis. Results from similar calculations at lower temperatures were published elsewhere [4].

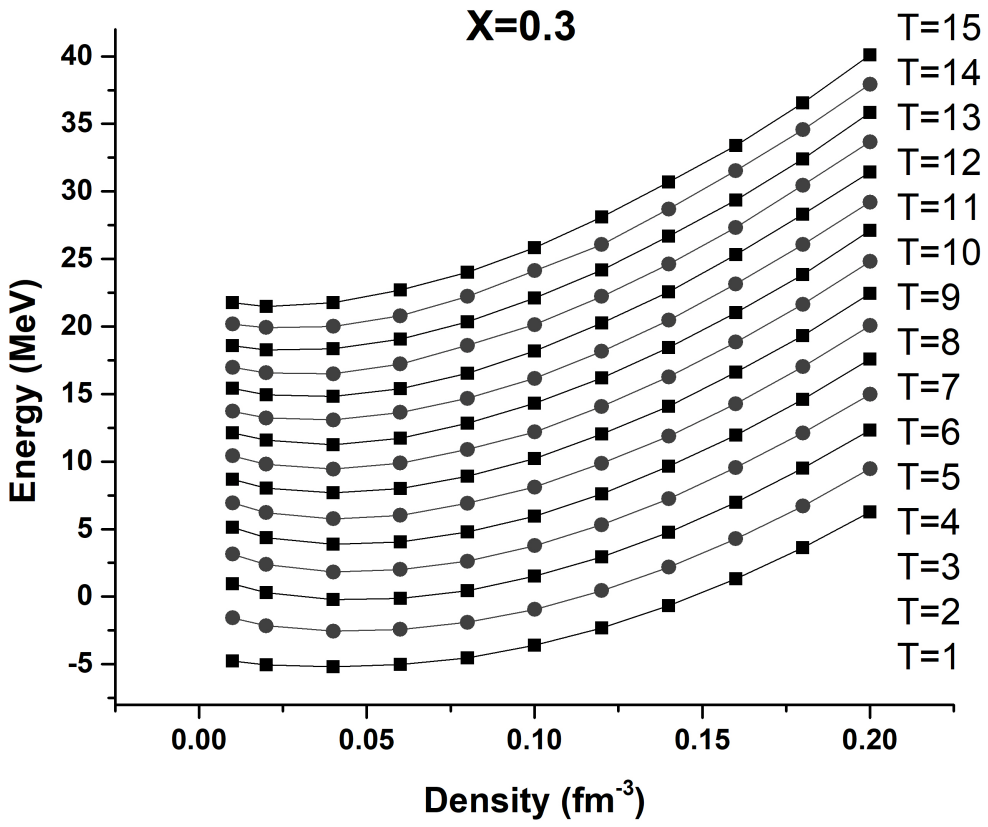

Figure 3.1: Plot for the average energy for $X = 0.3$ obtained using CMD simulations. The graph shows the characteristic $\cup$ shape for the density versus energy graphs that we have been observing in past studies.

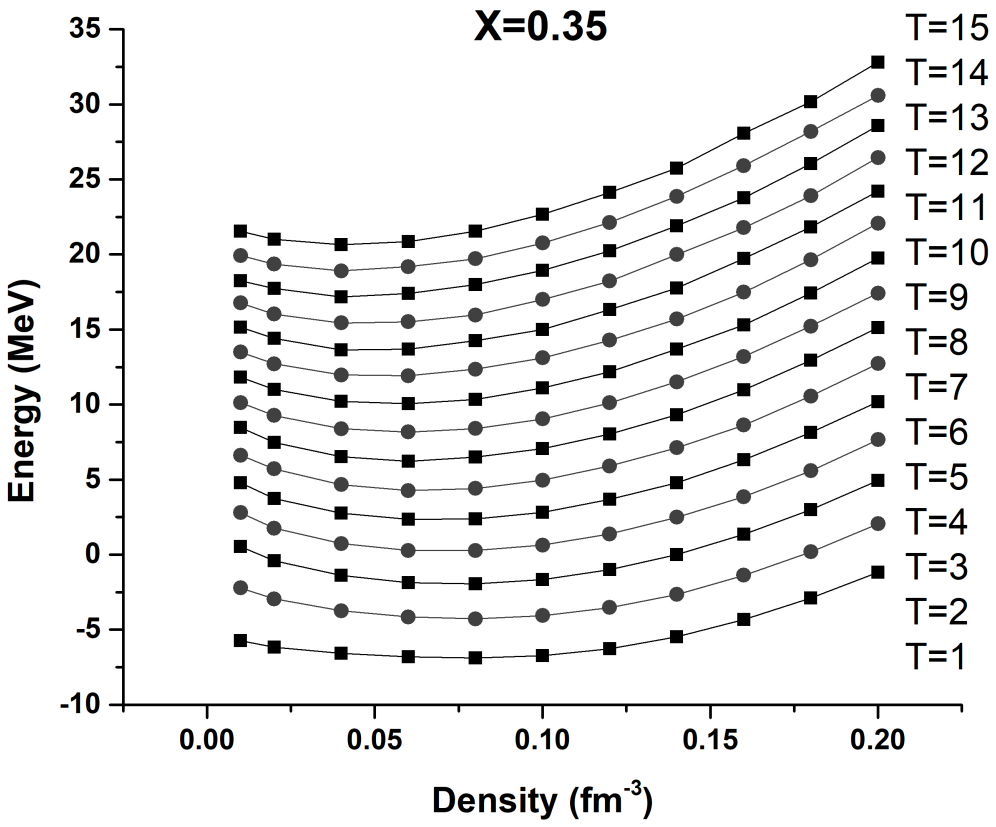

Figure 3.2: Plot for the average energy for $X = 0.35$ obtained using CMD simulations. The graph shows the characteristic $\cup$ shape for the density versus energy graphs that we have been observing in past studies.

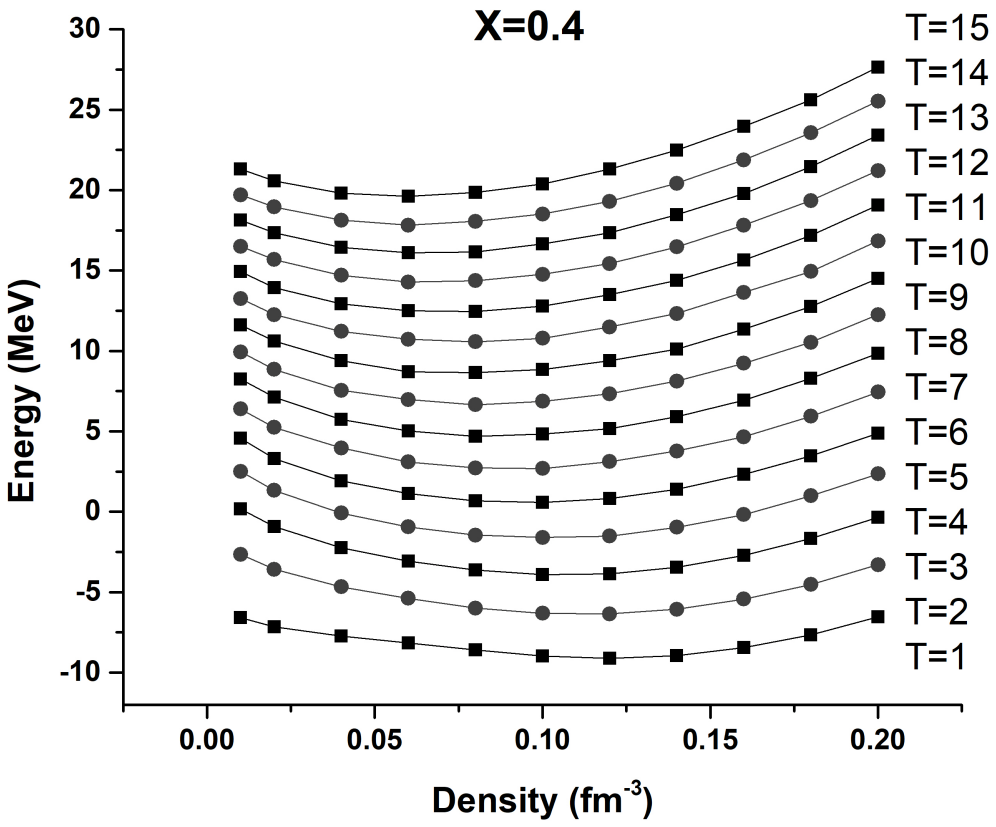

Figure 3.3: Plot for the average energy for $X = 0.4$ obtained using CMD simulations. The graph shows the characteristic $\cup$ shape for the density versus energy graphs that we have been observing in past studies.

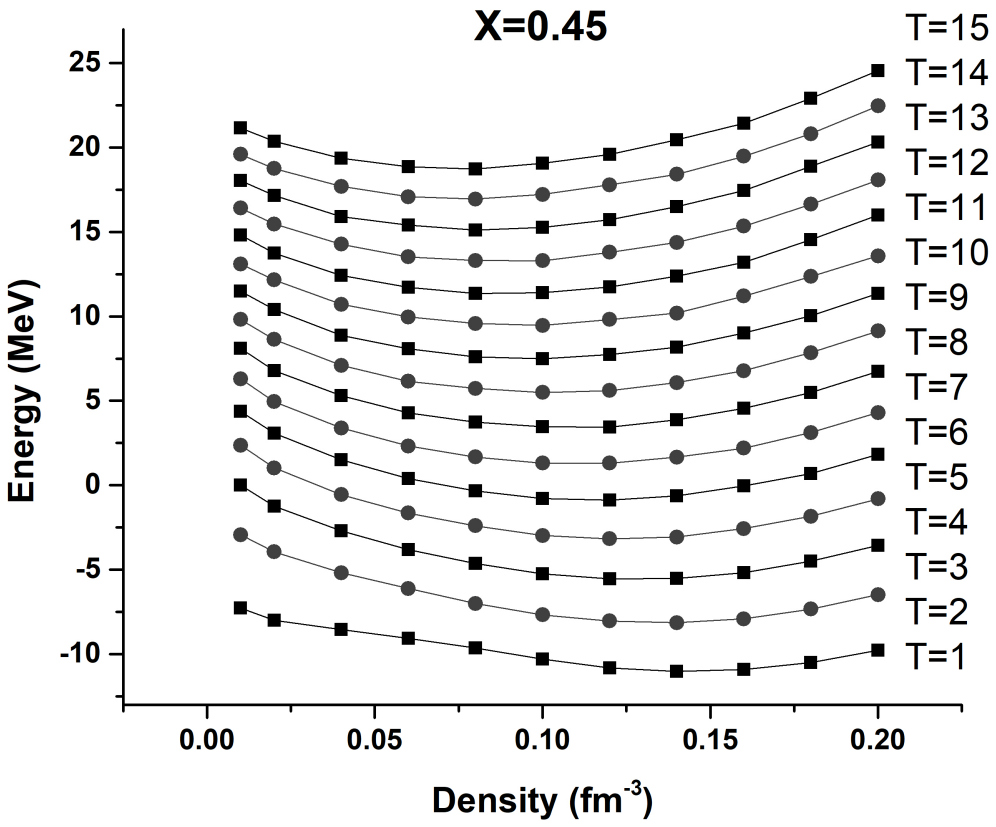

Figure 3.4: Plot for the average energy for $X = 0.45$ obtained using CMD simulations. The graph shows the characteristic $\cup$ shape for the density versus energy graphs that we have been observing in past studies.

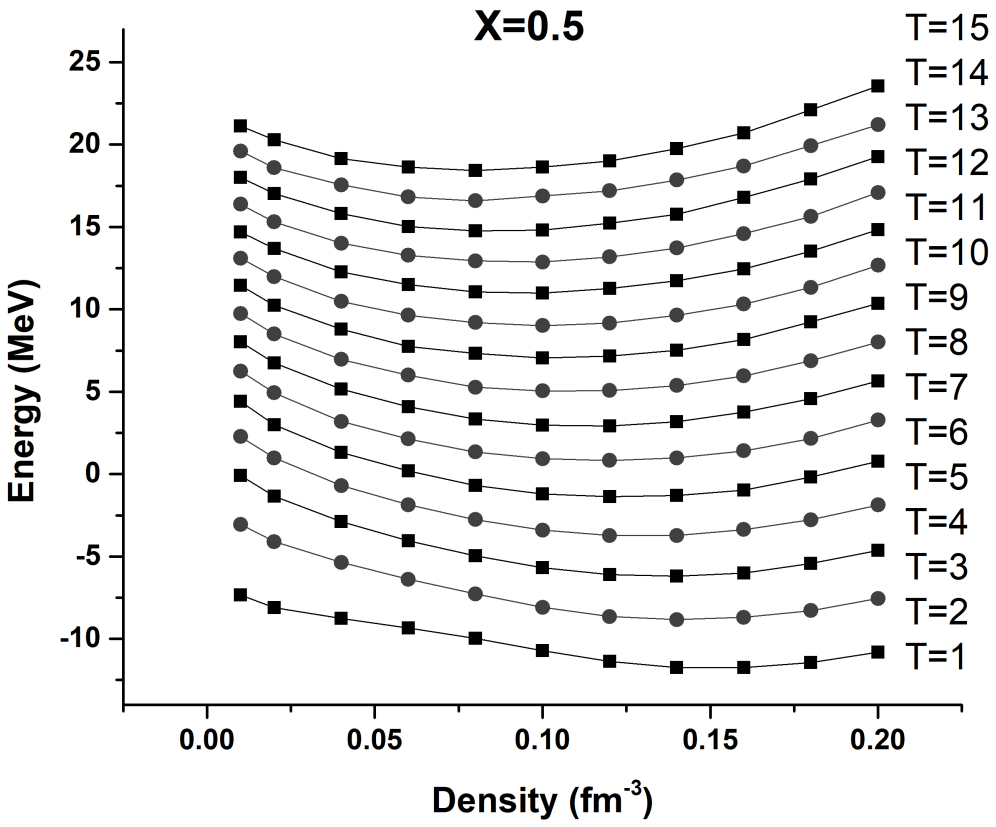

Figure 3.5: Plot for the average energy for $X = 0.5$ obtained using CMD simulations. The graph shows the characteristic $\cup$ shape for the density versus energy graphs that we have been observing in past studies.

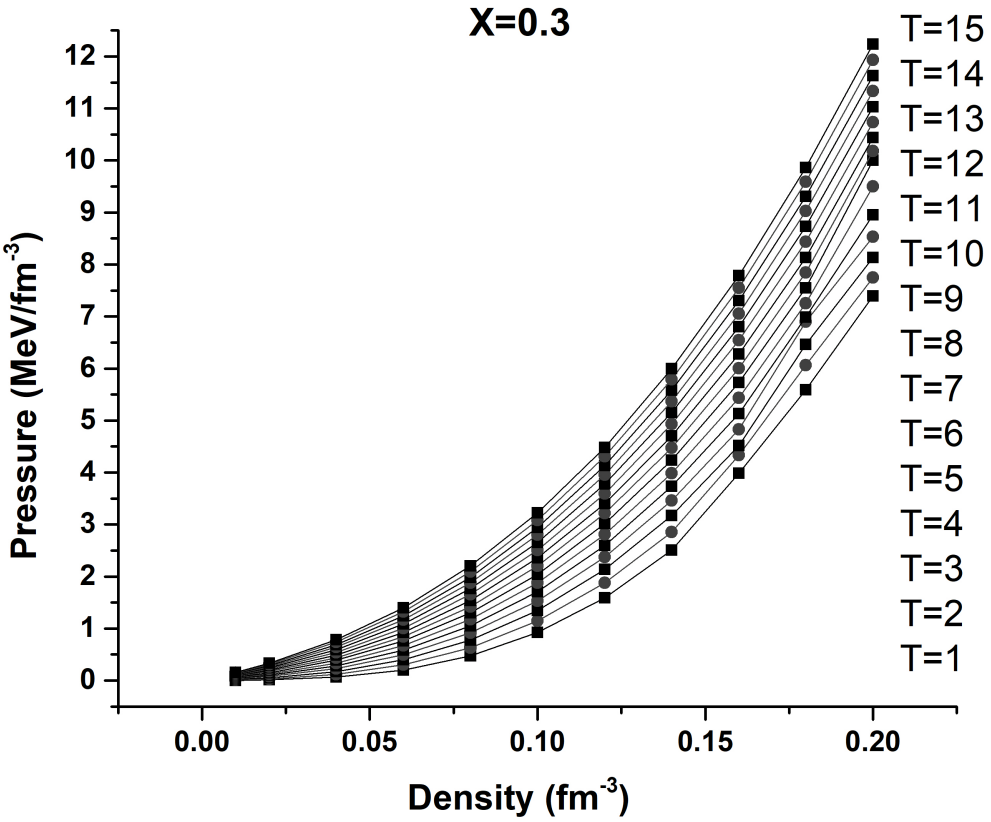

Figure 3.6: Plot for the average pressure for $X = 0.3$ obtained using CMD simulations.

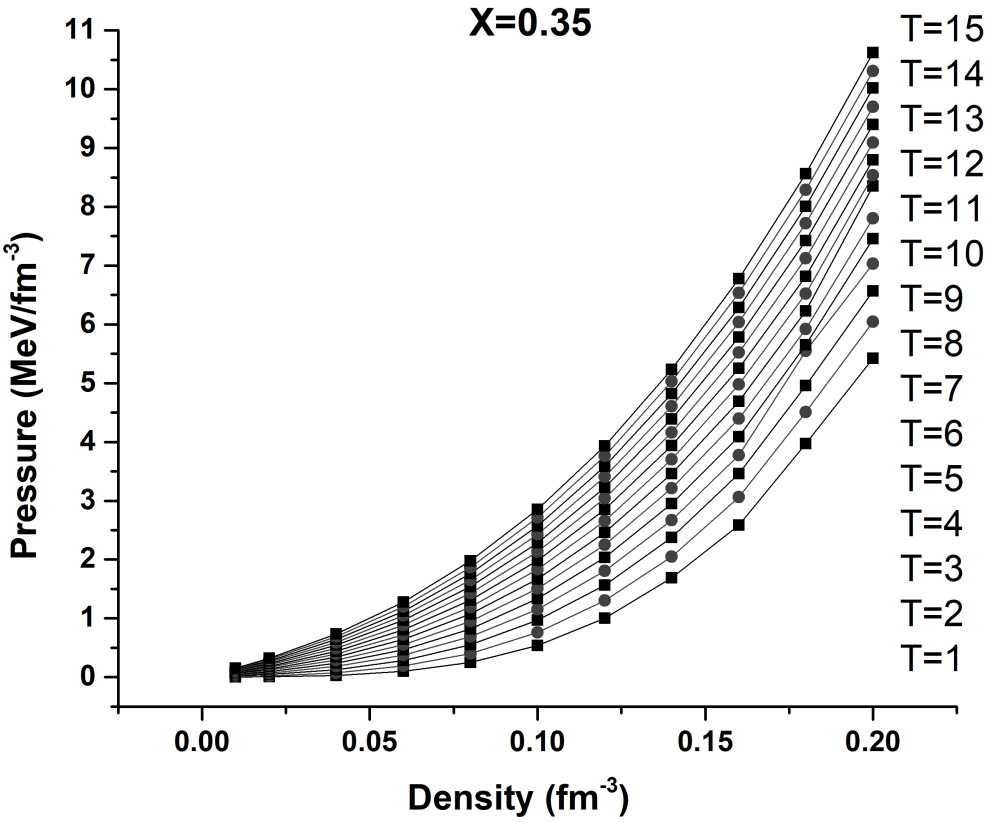

Figure 3.7: Plot for the average pressure for $X = 0.35$ obtained using CMD simulations.

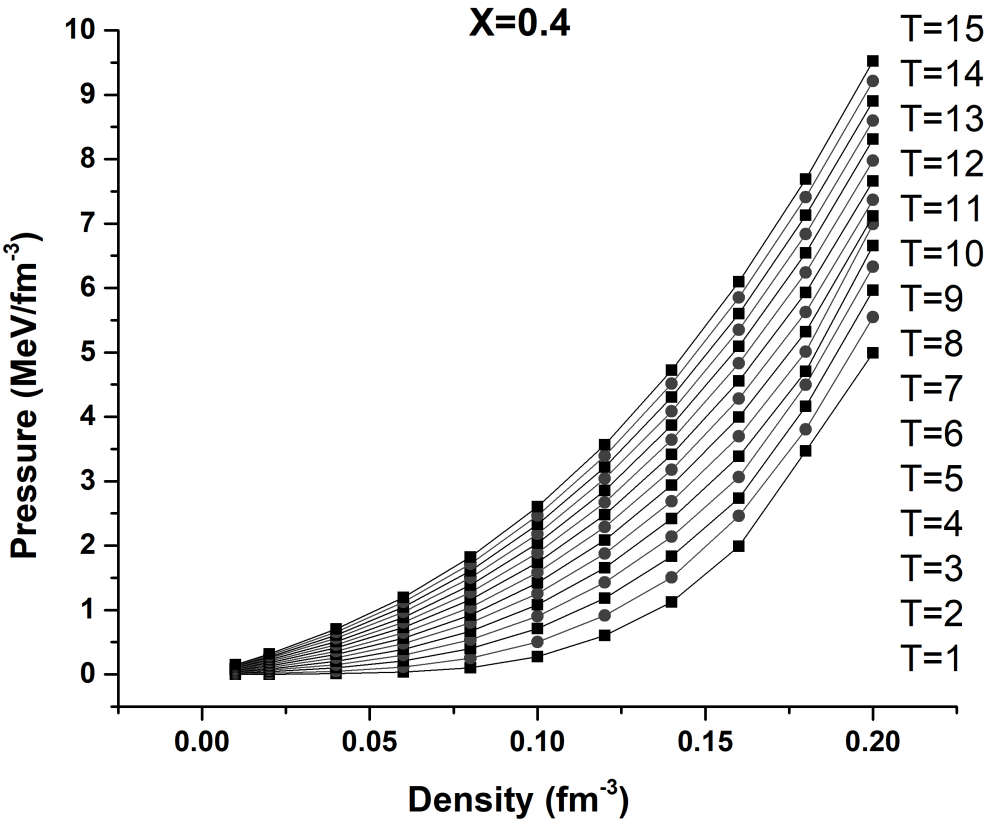

Figure 3.8: Plot for the average pressure for $X = 0.4$ obtained using CMD simulations.

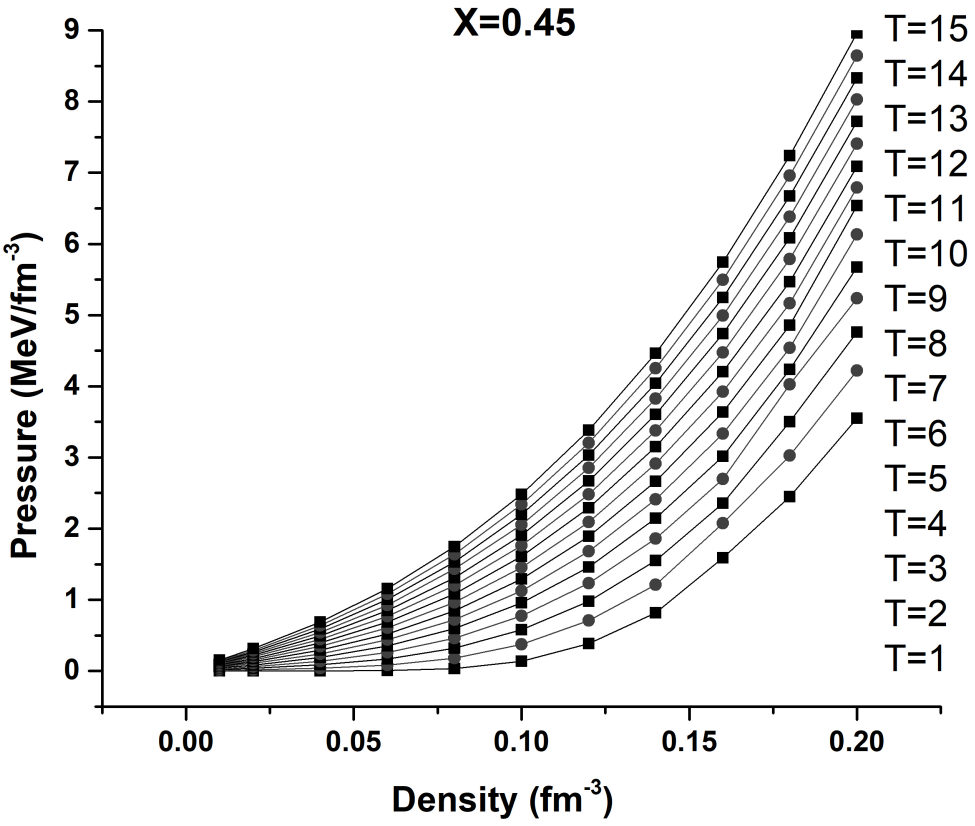

Figure 3.9: Plot for the average pressure for $X = 0.45$ obtained using CMD simulations.

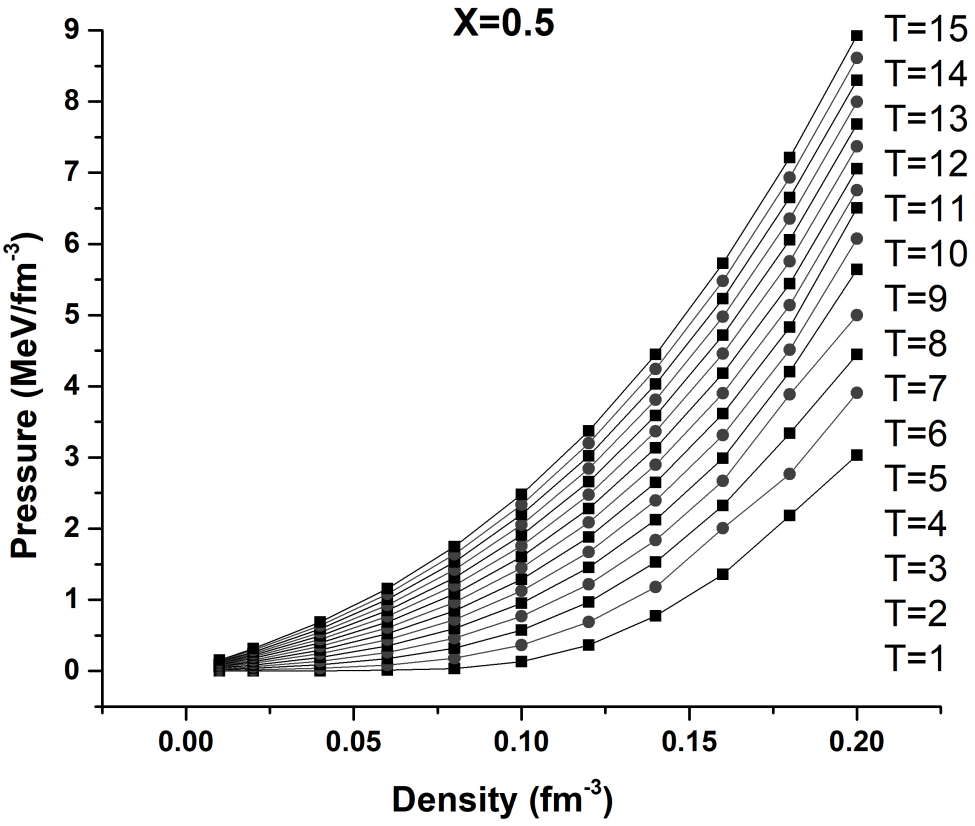

Figure 3.10: Plot for the average pressure for $X = 0.5$ obtained using CMD simulations.

Figures 3.11 and 3.12 show illustration of the energy and pressure for the cases $T = 1MeV$ and $11MeV$.

If we center our attention on figures 3.11(a) and 3.12(a), one could realize that they are full of physics; the equilibrium points for the liquid phase are the minima of the energy curves (maximum binding), the corresponding densities for those points are the liquid saturation densities and they vary with X decreasing for higher asymmetries. It is important to say that this behavior is expected to be found for all temperatures until we reach a critical temperature where the phase coexistence region ends.

Now, to extract the information from figures 3.11(a) and 3.12(a), the liquid phase can be identified by the section of the curve with a "$\cup$" shape; being the clearest case $X = 0.5$. Meanwhile, the points that deviate from the described "$\cup$" shape denote the existence of the liquid-gas mixture region, here we represent such points as empty symbols.

Another option to identify the liquid region is by their compressibility, that we can observe in figures 3.11(b) and 3.12(b), where the curvature of the pressure is $\partial p/\partial \rho > 0$.

The goal of the present study is to find the delimitations of the coexistence region. Although this has been sketched in the past for isospin symmetric matter [55, 56, 50] and evaluated for isospin asymmetric matter [57], this will be first time this is done dynamically with full inclusion of the isospin degree of freedom.

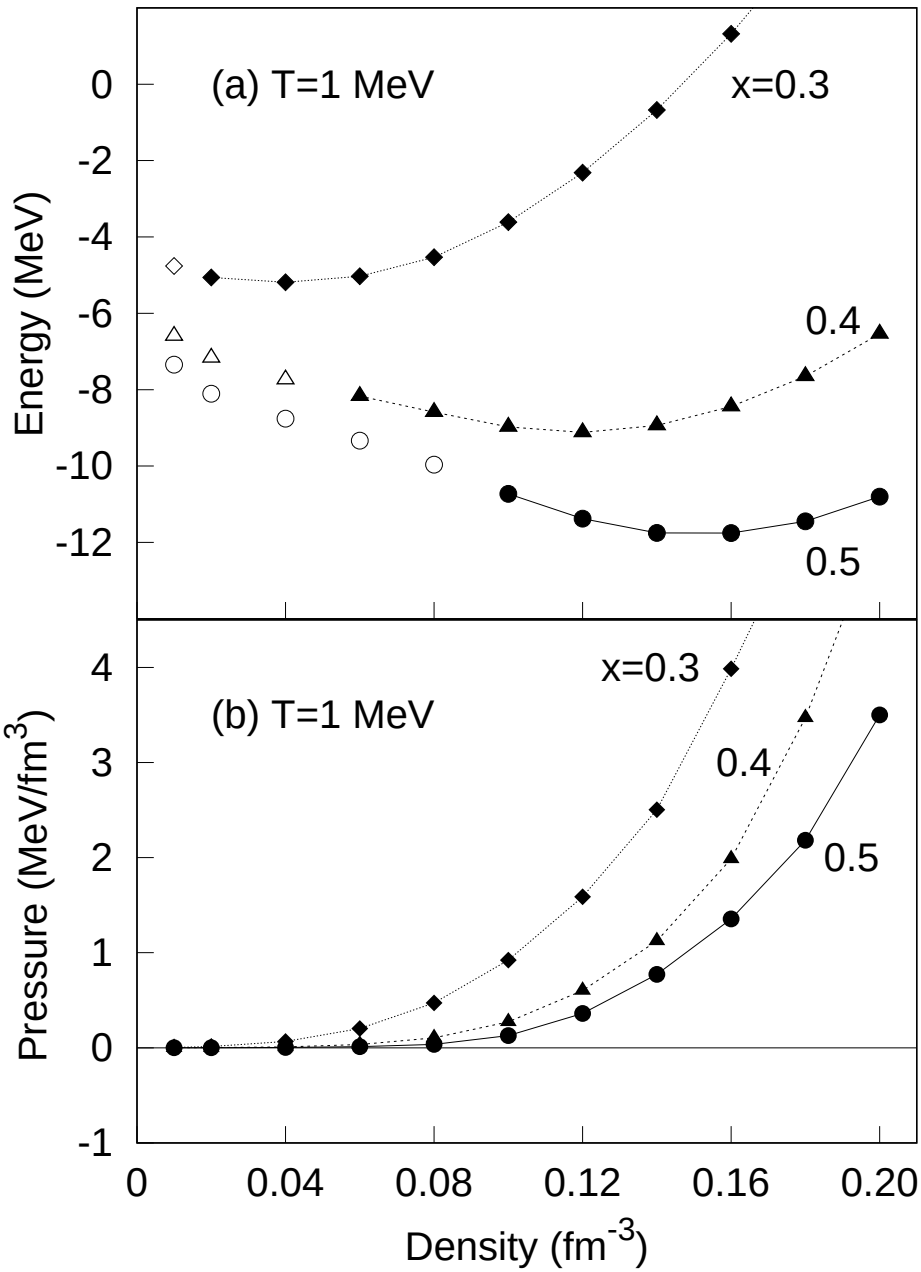

Figure 3.11: Energy per nucleon (a) and pressure (b) versus density for systems with $X = 0.3, 0.4$ and 0.5 at $T = 1MeV$.

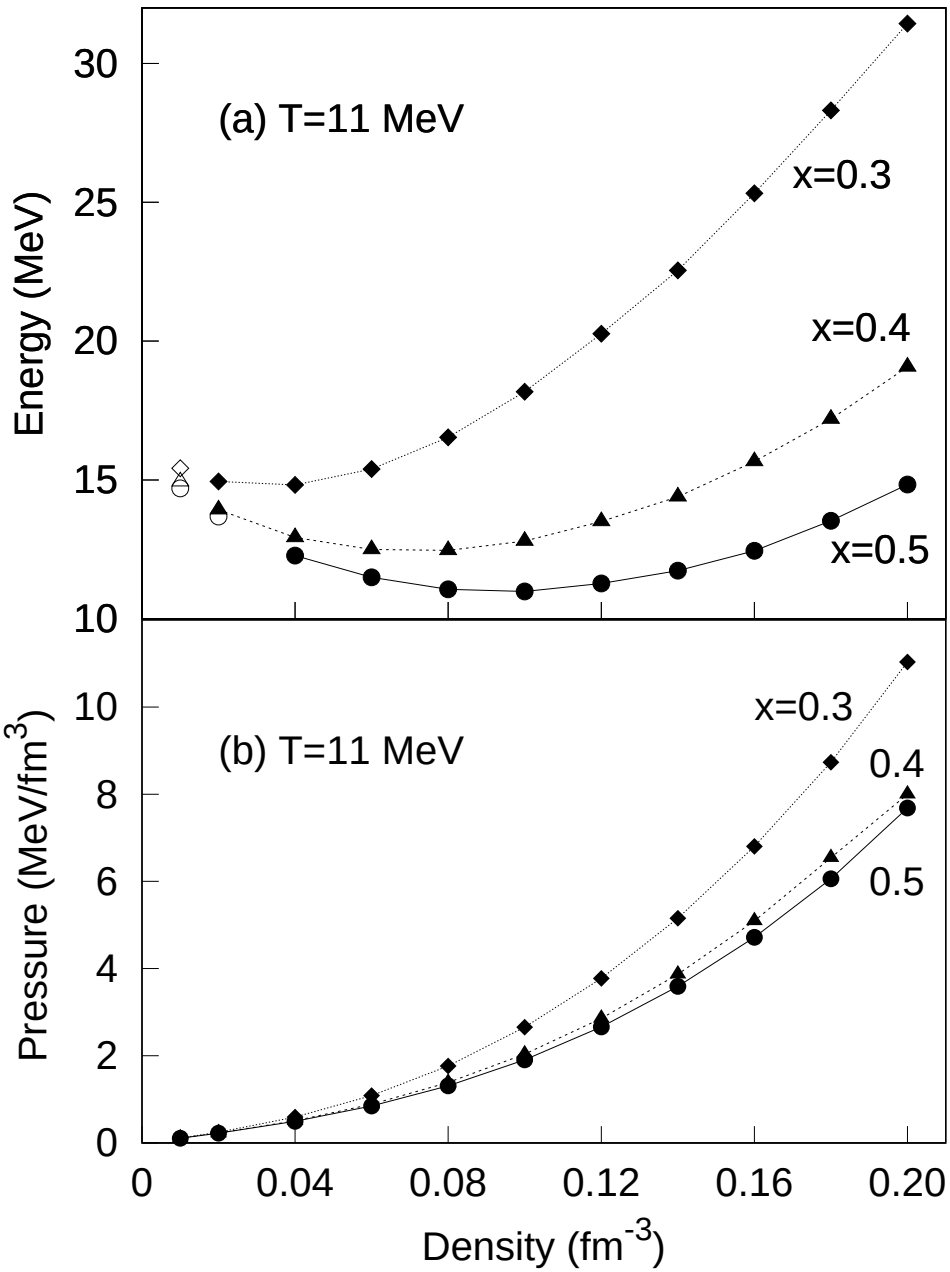

Figure 3.12: Same as Figure 3.11 for $T = 11MeV$.

Chapter 4

The Maxwell Construction

4.1 Complete Isotherms

To perform the Maxwell construction we need complete isotherms, to construct such curves we assume that at very low densities the pressure vs density isotherm is approximately the curve from a free nucleon gas, and around the saturation density the curves are given by CMD simulations, thus, a complete isotherm can be constructed by joining the gaseous segment with the liquid segment by an interpolation.

For the low-density gaseous part of the isotherm, we will use the pressure from a gas of nucleons approximation of a free Fermi gas $p(\rho, T) = \frac{2}{3}\rho\,\varepsilon_F(\rho, T)$ which, using the parametrization of the Fermi energy introduced in [56], can be approximated by

$$p(\rho, T) = \frac{\rho}{3}\sum_{i=2}^{5} i a_i (\rho/\rho_0)^{i/3+1} + \frac{2\rho}{3}\sum_{i=0}^{2}\varepsilon_i(T)\rho^i. \tag{4.1}$$

where $\varepsilon_i(T) = \sum_{j=1}^{2}\varepsilon_{ij}T^j$, and the coefficients ε_{ij} and a_i are listed in table 4.1.

The first term of Equation (4.1) approximates $2\rho/3$ times the Fermi energy of a cold nucleon gas, and the second term approximates $2\rho/3$ times the T-dependent Fermi gas energy. It is important to mention that, as we expected, at low densities, equation (4.1) does not depend on the isospin content X, as the system is highly noninteracting.

We will use the obtained approximation in the low-density gaseous region ($\rho \leq \rho_0/6$), and the CMD data curves for the liquid phase (from $\rho \geq \rho_L$, where ρ_L refers to the luquid saturation density), and as we said, we will join both segments of curve by a least-squares cubic interpolation that matches the three segments and their first derivatives (to guarantee smoothness in the connections) to construct the complete isotherm. Figure 4.1

Table 4.1: Coefficients ε_{ij}^{T} and a_i

Coefficient	Value	Coefficient	Value
ε_{01}	0.693	ε_{02}	$0.037MeV^{-1}$
ε_{11}	-5.420	ε_{12}	$0.082MeV^{-1}$
ε_{21}	11.447	ε_{22}	$-0.312MeV^{-1}$
a_2	$21.1MeV$	a_3	$-38.3MeV$
a_4	$-26.7MeV$	a_5	$35.9MeV$

shows one example of a resulting pressure-density curve; the values used for the matching liquid density ρ_L vary depending on the values of T and X.

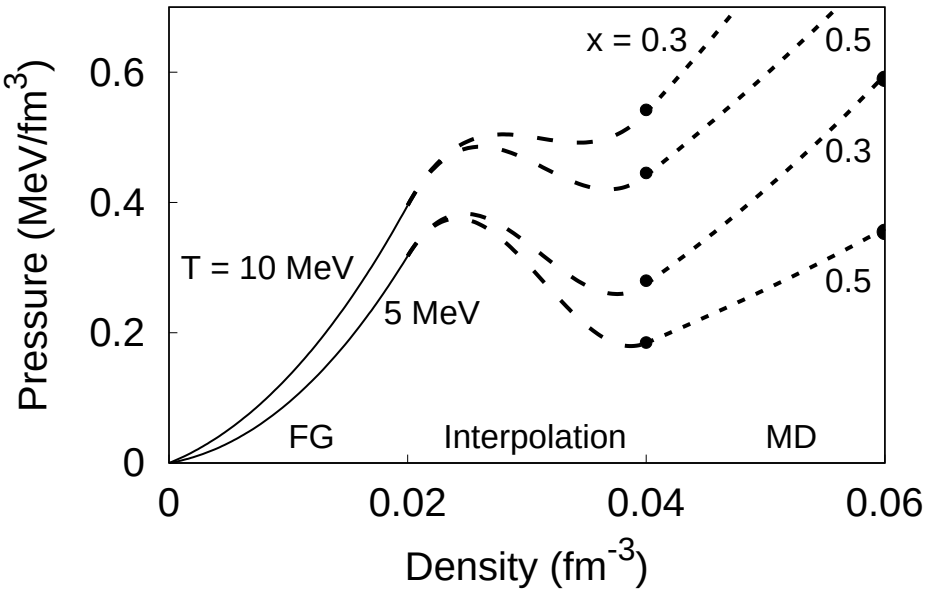

Figure 4.1: Example of pressure density interpolated curves for the cases of $T = 5$ and $10MeV$, $X = 0.3$ and 0.5. "FG" stands for Fermi gas, located on the left-hand side of the curve (continuous line) and obtained with equation 4.1, "MD" indicates the right-hand side segments (short dashes) and corresponds to the fit to the molecular dynamics results, and "Interpolation" refers to the middle segment obtained by a least-squares cubic interpolation to match the FG and MD segments. The points indicate MD-calculated points.

4.2 Maxwell Construction

To determine the region of liquid-gas coexistence we use the Maxwell construction. In summary, the conditions of equilibrium lead to a mathematical identity for the Gibbs free energy, which in turn allows the calculation of the equilibrium pressure and the boundaries of the coexistence region.

The conditions for thermal, mechanical and chemical equilibrium between a liquid and a gaseous phases are that both phases must maintain the same temperature, pressure and chemical potential, namely $T_{liquid} = T_{gas}$, $p_{liquid} = p_{gas}$ and $\mu_{liquid} = \mu_{gas}$; this last condition is related to the Gibbs free energy.

The Gibbs free energy is defined in terms of the internal energy U: $G = U + pV - TS$, and since $U = TS - pV + \mu N$, we get that $G = \mu N$, which indicates that equilibrium will be achieved when $G_{liquid} = G_{gas}$. To find such point it is convenient to plot G as a function of p. Although G is not calculated in this thesis, its behavior as a function of p generally looks as figure 4.2 [56].

In physical terms, the segment from before point A and up to C shows the Gibbs free energy the system has in the gaseous phase, and the segment G to I and beyond is for the liquid phase. The segment $C - D$ corresponds to supercooled vapor and $F - C$ to superheated liquid, both metastable, and $D - F$ is an unstable region. It is clear that the only stable point where the equilibrium condition, $\mu_{liquid} = \mu_{gas}$, is met is at points C and G where $G_{liquid} = G_{gas}$. Determining such crossing point would determine the equilibrium pressure uniquely.

To determine the exact location of the point C or G we observe that a medium that traverses the loop $C - D - F - G$ will end up with the same amount of free energy it had at the start, i.e. $\Delta G|_{CDFG} = 0$. To evaluate such change we remember that an infinitesimal change is

$$dG = dU + pdV + Vdp - TdS - SdT,$$

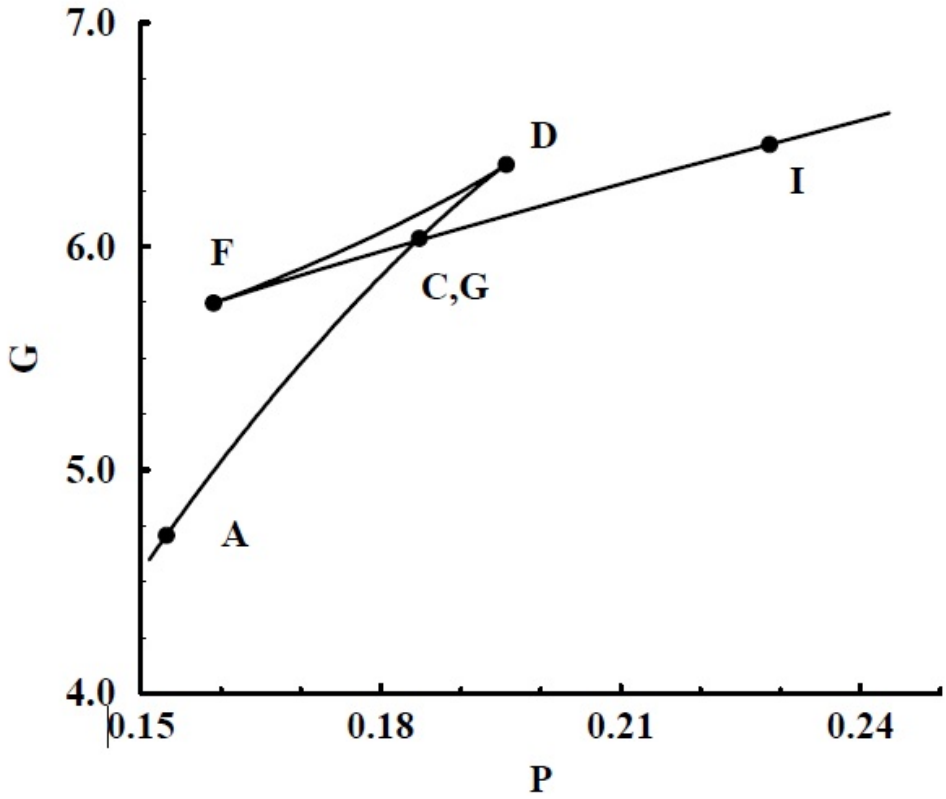

Figure 4.2: Gibbs free energy G as a function of pressure p for an isotherm below the critical temperature T_c

and since $dU = TdS - pdV + \mu dN$ this becomes

$$dG = Vdp - SdT + \mu dN,$$

but since $dG = (\partial G/\partial p)_{T,N}dp + (\partial G/\partial T)_{p,N}dT + (\partial G/\partial N)_{T,p}dN$, we get

$$(\partial G/\partial p)_{T,N} = V,\ (\partial G/\partial T)_{p,N} = -S \text{ and } (\partial G/\partial N)_{T,p} = \mu. \tag{4.2}$$

Since we are keeping constant the temperature and N, we focus on the first of the equalities (4.2):

$$(\partial G/\partial p)_{T,N} = V \implies \Delta G = \int_C^G Vdp = 0 \tag{4.3}$$

To evaluate the integral 4.3 we study the plot of $V(p)$; figure 4.3 shows the case of the isotherm for $T = 9\ MeV$ and $X = 0.4$.

In Figure 4.3 the gaseous phase corresponds to all points before C, the coexistence arc to those between C and G, and the liquid phase to all points beyond G. The arc where $dV/dp > 0$ (points between D and F) is unstable to any density fluctuation. The portion of the isotherms from the boundary of the coexistence curve to the limits of the unstable spinodal region are physically accessible, albeit momentarily, and are called the *superheated vapor* (points between C and D) and *supercooled liquid* (points between F and G.)

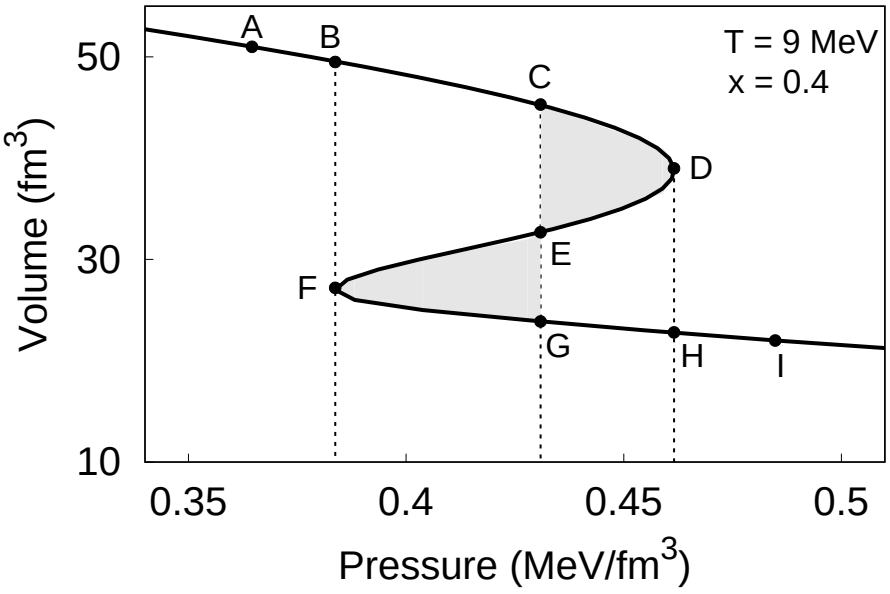

Figure 4.3: Pressure Isotherm for $T = 9MeV$ and $X = 0.4$ plotted sideways versus the volume. The shaded area to the right of the dotted line C-G and the curve C-D-E equals the area to the left of the dotted line and the curve E-F-G. The liquid-gas coexistence region is limited by volumes V_C and V_G, and the unstable region lies between volumes V_D and V_F.

Integral (4.3) then becomes

$$\int_{CDEFG} V(p)dp = \int_{CD} V(p)dp - \int_{DE} V(p)dp - \int_{EF} V(p)dp + \int_{FG} V(p)dp = 0 \qquad (4.4)$$

which implies that

$$\int_{CD} Vdp - \int_{DE} Vdp = \int_{EF} Vdp - \int_{FG} Vdp \qquad (4.5)$$

Which in turn indicates that the areas determined by the vertical straight line of constant pressure p (going through points C, E and G) and the isotherm under study, to the left and the right of the intersect in the unstable region, must be equal. Finding the pressure at which those two areas are equal to each other is known as the "Maxwell Construction", and it is used to determine i) the equilibrium pressure, and ii) the boundaries of the coexistence curve, i.e. the corresponding volumes, V_C and V_G.

In practice the Maxwell Construction is carried out numerically by finding the pressure at which $\int_{V_C}^{V_G} pdV = 0$ for each isotherm; once the pressure is known it automatically yields V_C and V_G; appendix B contains a Mathematica routine to evaluate this procedure.

To determine the boundary points of the whole coexistence region it is necessary to apply this Maxwell construction method to all the cases in our study, this is, a total of 75 times. Figure 4.4 shows three pressure isotherms plotted versus the volume for the cases $T = 1$, 10 and $15MeV$ and for $X = 0.35$. The continuous curves of the left show a fit to the CMD results (points), and the dashed curves of the right are the least square fits inverted to appear as a function of the volume. The coexistence region is obtained by repeatedly integrating the area between a given pressure value and the pressure isotherm, until the pressure at which the integral is zero is found. The resulting pressures for the cases $T = 1$ and $10MeV$ are indicated with the horizontal lines; for the case of $T = 15MeV$ no pressure satisfied the condition of zero integral indicating that for $X = 0.35$ the coexistence region ends at a lower temperature.

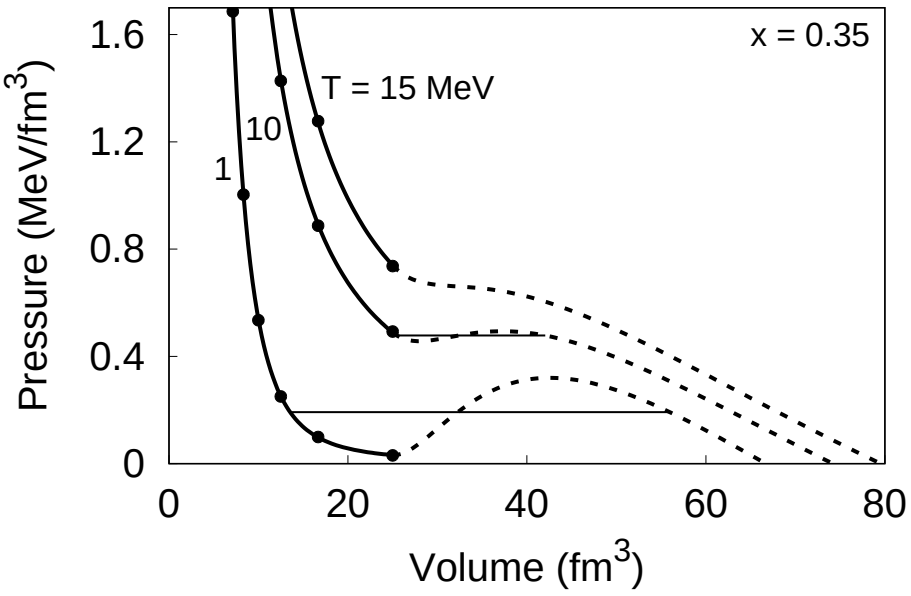

Figure 4.4: Pressure isotherms for $T = 1$, 10 and $15MeV$ and $X = 0.35$. The points are the CMD results, the continuous curves are fits to such results, and the dashed curves are the cubic least square fits. The pressures at which $g = \int_{V_{Liq}}^{V_{Gas}} V \, \mathrm{d}p = 0$ are shown (horizontal lines) for the cases $T = 1$ and $10MeV$; at $T = 15MeV$ nuclear matter at $X = 0.35$ never reaches a liquid-gas mix phase.

Chapter 5

The Phase Diagram

After we applied the Maxwell construction for all our cases, we got two values of density ρ_{Liq} and ρ_{Gas}, which delimitate the phase coexistence region for each of the individual cases. There are several cases where we were not able to get such density values, this is because the coexistence region tends to disappear for asymmetric nuclear matter at high temperatures.

On tables 5.1 and 5.2 we list for all the cases that we worked, the initial density where the phase coexistence region begins as ρ_{Gas}, and the last density where such region ends as ρ_{Liq}. The spaces in blank inside the tables correspond to the cases where the phase coexistence region disappears.

Temperature T	$X = 0.5$		$X = 0.45$		$X = 0.4$	
	ρ_{Gas}	ρ_{Liq}	ρ_{Gas}	ρ_{Liq}	ρ_{Gas}	ρ_{Liq}
$T = 1$	0.0172952	0.103496	0.0172759	0.102106	0.0174856	0.0896282
$T = 2$	0.0177649	0.0821142	0.017749	0.0819108	0.0179559	0.0731937
$T = 3$	0.0179833	0.064122	0.0182973	0.0692462	0.0184892	0.0640718
$T = 4$	0.0187425	0.0571258	0.0187307	0.0572324	0.0189015	0.0544435
$T = 5$	0.0193743	0.0534634	0.0193518	0.0535684	0.0195647	0.0514435
$T = 6$	0.0195024	0.0477828	0.0194798	0.047816	0.0196799	0.0467042
$T = 7$	0.020331	0.0461789	0.0202925	0.046198	0.02053	0.0451352
$T = 8$	0.0210552	0.044305	0.0210676	0.0443702	0.0213164	0.0433816
$T = 9$	0.0217928	0.0426258	0.021775	0.0426424	0.0221017	0.0418684
$T = 10$	0.0226099	0.0412351	0.0226106	0.0412836	0.0229829	0.0405883
$T = 11$	0.0234831	0.0400937	0.0234322	0.0401447	0.0240483	0.0395036
$T = 12$	0.0244019	0.0391836	0.0243304	0.0391819	0.0249838	0.0386945
$T = 13$	0.0256057	0.0384858	0.0254483	0.038441	0.026417	0.0380719
$T = 14$	0.0269367	0.0379123	0.0268907	0.03793	0.0286876	0.0375824
$T = 15$	0.0293301	0.0375117	0.0293067	0.0375351	–	–

Table 5.1: Values of density (fm^{-3}) that delimitate the phase coexistence region for each temperature T (MeV).

Temperature T	$X = 0.35$		$X = 0.3$	
	ρ_{Gas}	ρ_{Liq}	ρ_{Gas}	ρ_{Liq}
$T = 1$	0.0178656	0.073841	0.0183724	0.0614397
$T = 2$	0.0183023	0.0615306	0.0187915	0.0532862
$T = 3$	0.0188889	0.0570436	0.0194957	0.0506966
$T = 4$	0.0191471	0.0495062	0.0196703	0.0459223
$T = 5$	0.0199495	0.0478285	0.0206311	0.0443808
$T = 6$	0.0207041	0.0455759	0.0215489	0.0426095
$T = 7$	0.0208091	0.0431495	0.0216161	0.0410875
$T = 8$	0.0218055	0.0417506	0.0228773	0.0398652
$T = 9$	0.0227627	0.0404584	0.0241932	0.0388194
$T = 10$	0.0237867	0.0393539	0.0259145	0.0379845
$T = 11$	0.025056	0.0385276	0.0289724	0.0373101
$T = 12$	0.0267483	0.0378612	–	–
$T = 13$	–	–	–	–
$T = 14$	–	–	–	–
$T = 15$	–	–	–	–

Table 5.2: Values of density (fm^{-3}) that delimitate the phase coexistence region for each temperature T (MeV).

5.1 2 -Dimensional Phase Diagrams

Using the values showed on tables 5.1 and 5.2, we can construct a phase diagram for each proportion X, on such a manner that we can see with more clarity the necessary conditions where our system is on the gas phase region, the liquid phase region, or the phase coexistence region. These diagrams are in function of density and temperature, see figures 5.1, 5.2, 5.3, 5.4, and 5.5.

To have an approximate limit of the coexistence region, we performed an interpolation of the values in both tables with a polynomial function of 3th grade, plotted only in our interval of interest. Here, the highest point of the interpolation is defined as "critical temperature"; this is the approximate value of temperature where the coexistence of phases region disappears for each of the proportions X.

The left-hand side of the phase diagrams correspond to the gas region, the right-hand side to the liquid region, and the area below the curve correspond to the phase coexistence region.

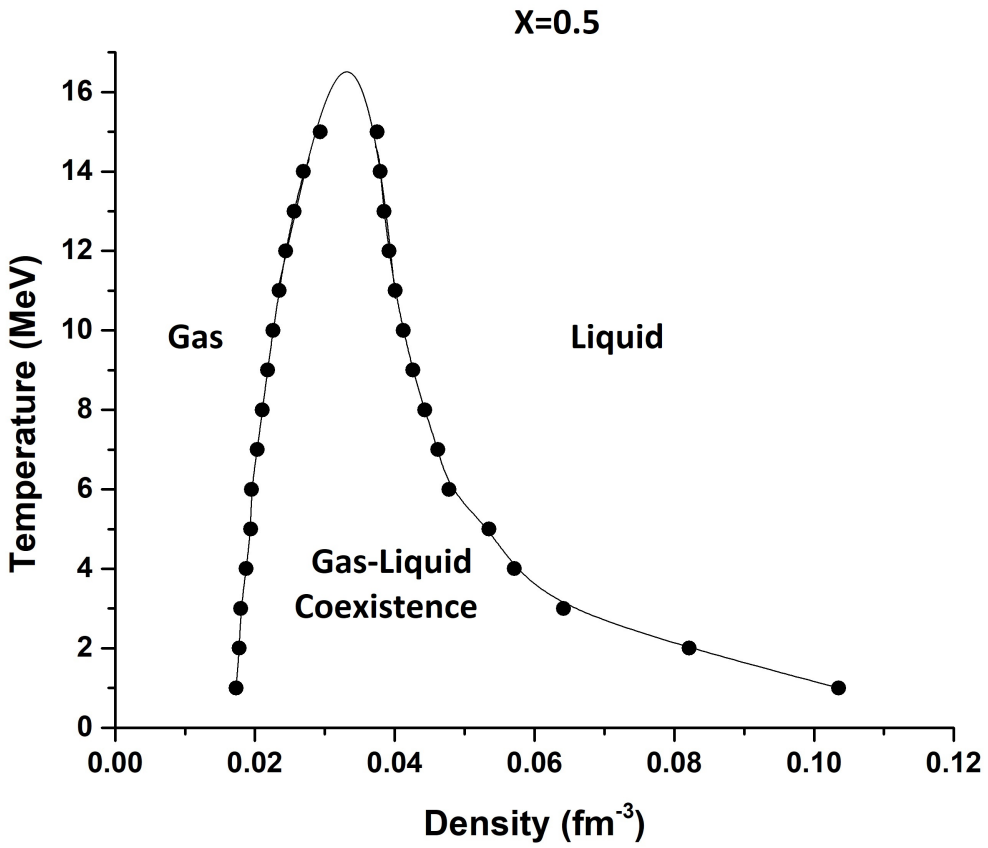

Figure 5.1: Phase diagram with the values of ρ_{Gas} and ρ_{Liq} for the case $X = 0.5$, in the left-hand side of the highest peak in the plot we have the gaseous phase, on the right-hand side we have the liquid phase, and in the area below the curve we have the phase coexistence region.

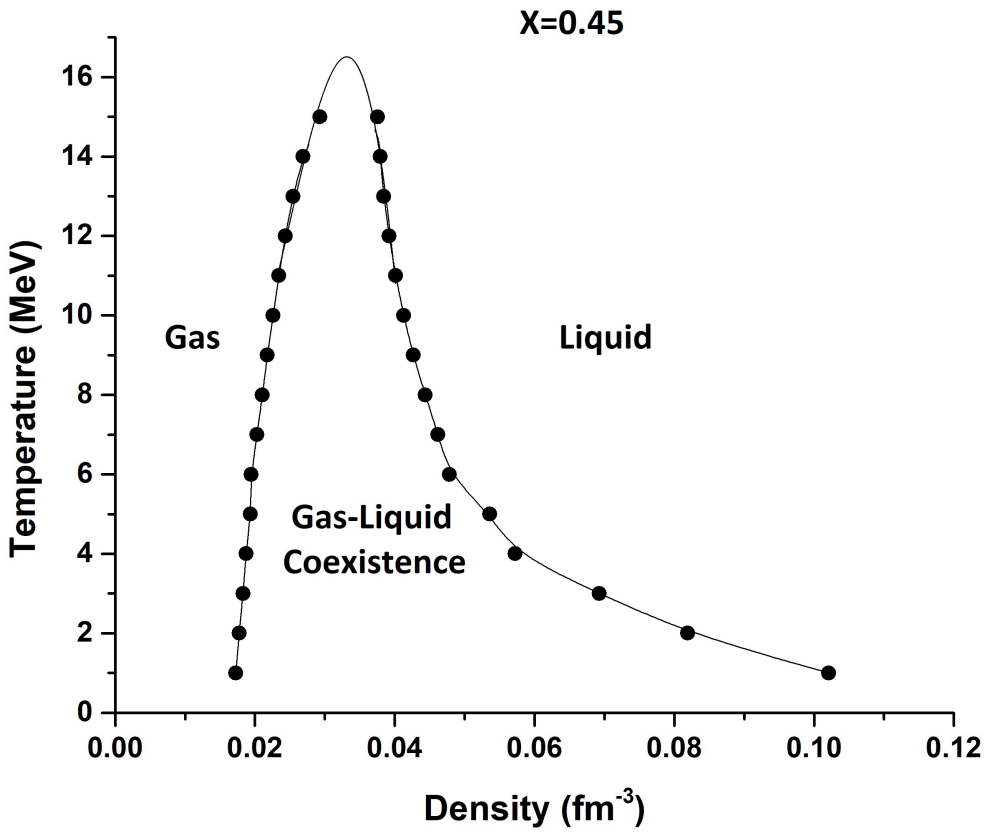

Figure 5.2: Phase diagram with the values of ρ_{Gas} and ρ_{Liq} for the case $X = 0.45$, in the left-hand side of the highest peak in the plot we have the gaseous phase, on the right-hand side we have the liquid phase, and in the area below the curve we have the phase coexistence region.

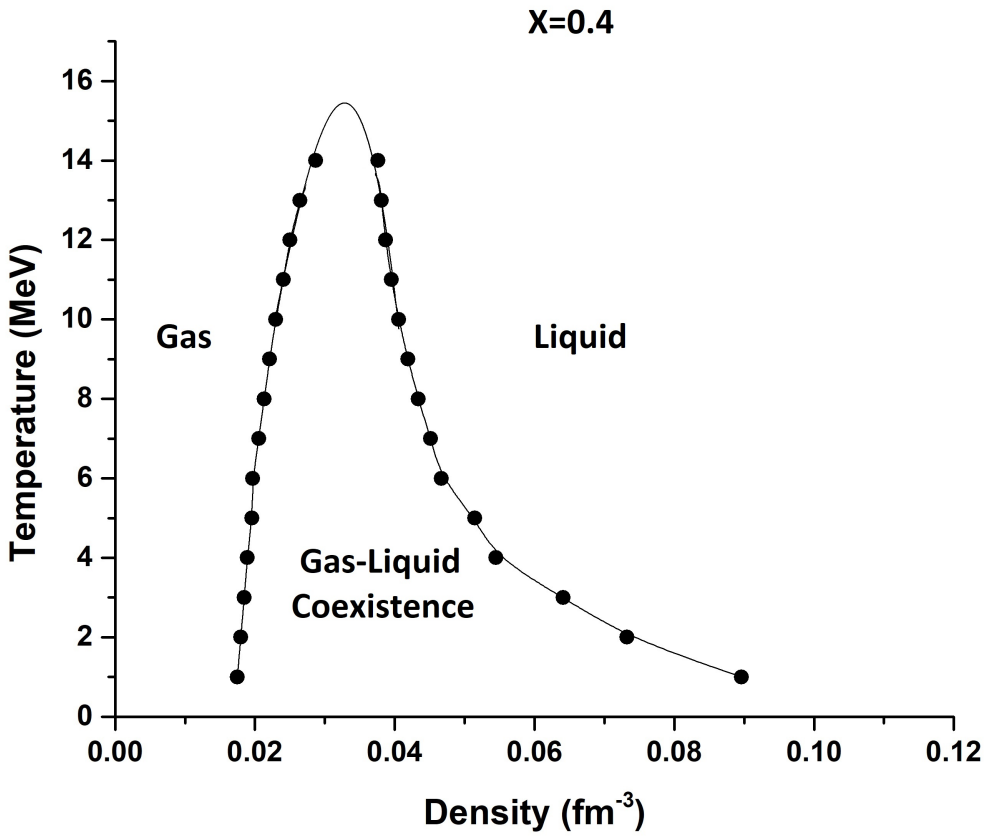

Figure 5.3: Phase diagram with the values of ρ_{Gas} and ρ_{Liq} for the case $X = 0.4$, in the left-hand side of the highest peak in the plot we have the gaseous phase, on the right-hand side we have the liquid phase, and in the area below the curve we have the phase coexistence region.

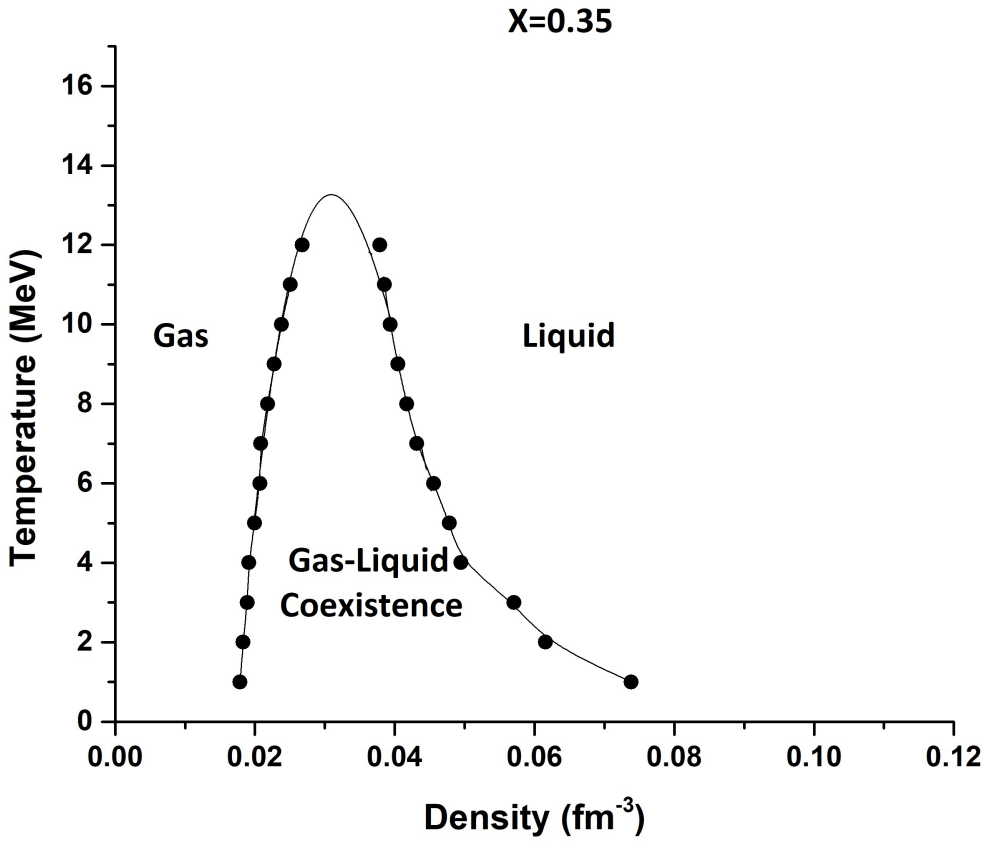

Figure 5.4: Phase diagram with the values of ρ_{Gas} and ρ_{Liq} for the case $X = 0.35$, in the left-hand side of the highest peak in the plot we have the gaseous phase, on the right-hand side we have the liquid phase, and in the area below the curve we have the phase coexistence region.

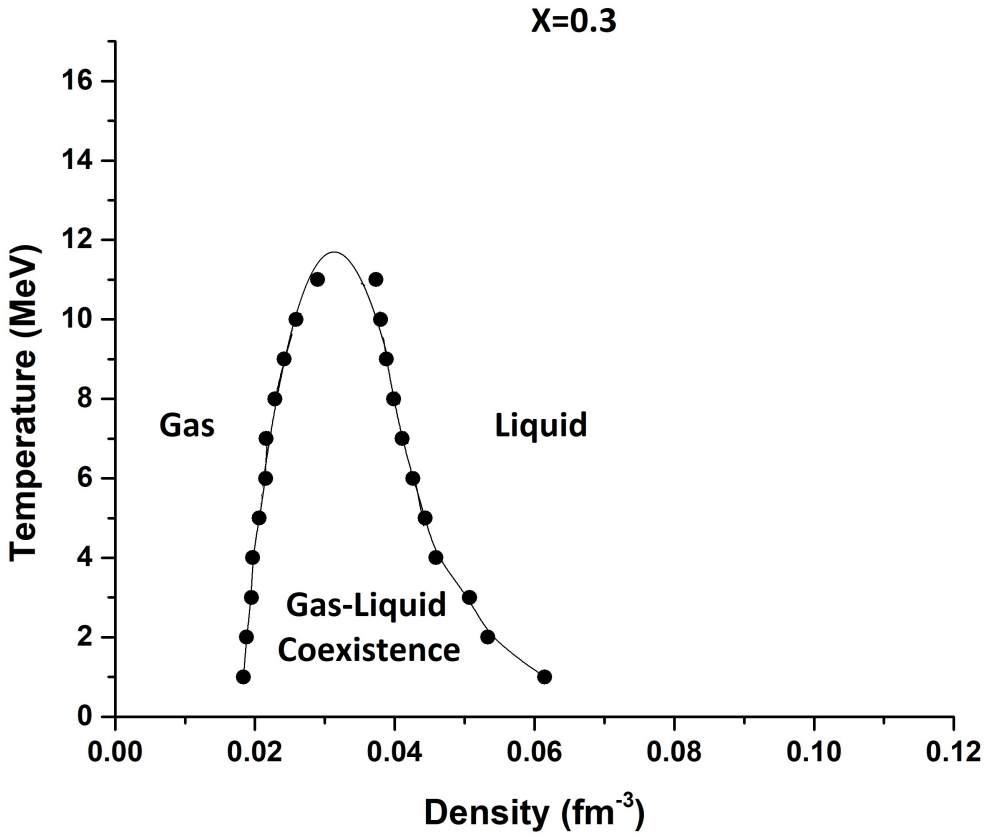

Figure 5.5: Phase diagram with the values of ρ_{Gas} and ρ_{Liq} for the case $X = 0.3$, in the left-hand side of the highest peak in the plot we have the gaseous phase, on the right-hand side we have the liquid phase, and in the area below the curve we have the phase coexistence region.

5.2 Phase Diagram

At this point, it is clear to see that we can obtain a two-dimensional phase diagram for each of the different isospin content cases $X = 0.3$, 0.35, 0.4, 0.45 and 0.5. Now, such two-dimensional phase diagrams can be combined in a three-dimensional phase diagram in the *density-X-temperature* space as shown in figure 5.6. The generated surface was obtained using the software *Mathematica* with the instruction *ListPlot*3*D*, which approximate the obtained 2-D diagrams to fit a surface that joins the array of *temperature-density-X* points. The volume under the surface is the liquid-gas coexistence region generalized into the proton fraction X axis.

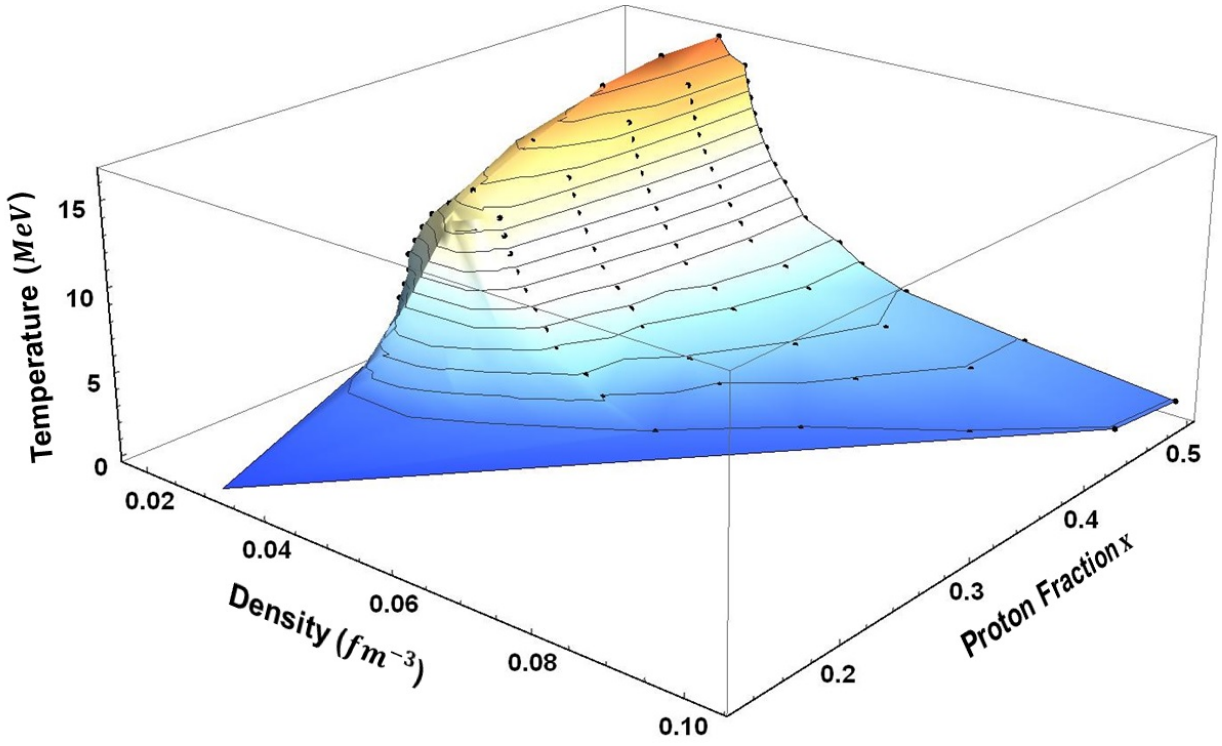

Figure 5.6: *Density-X-Temperature* phase diagram. The liquid-gas coexistence region is the volume under the surface. The points are the density-temperature points obtained from the Maxwell construction for the various values of X [60].

Approximately the surface on 5.6 closes at a value of X less than 0.3, this was found by an extrapolation of the trend of the critical temperatures we already have because of the lack of information for smaller values of X. However, from CMD we know that for lower values of X the systems are unbound almost for all temperatures, which means that the Maxwell construction process cannot be applied anymore (as in the case $T = 15MeV$ for $X = 0.35$, see figure 4.4)

Now, on figure 5.7 we can see how the critical temperatures decline for lower values of X. The points in the figure show the critical temperatures obtained from the maxima of the fits used in figures 5.1, 5.2, 5.3, 5.4, and 5.5 for all values of X. The continuous line is a parabolic fit, which has been extended to lower values of X with an artistic touch in the background indicating the region where bubbles and droplets coexist. As the curve reaches the $T = 0$ value at $X = 0.1324$, we conclude that such point is the lower X limit of the liquid-gas mix region, and that outside of this ρ-T-X volume all nuclear systems are expected to be fully unbound. Although this coexistence region has never been calculated before, our findings are in general agreement with the low binding energy of $X = 0.3$ matter found in [58], and of unbound pure neutron matter ($X = 0$) found in [59] at zero temperature.

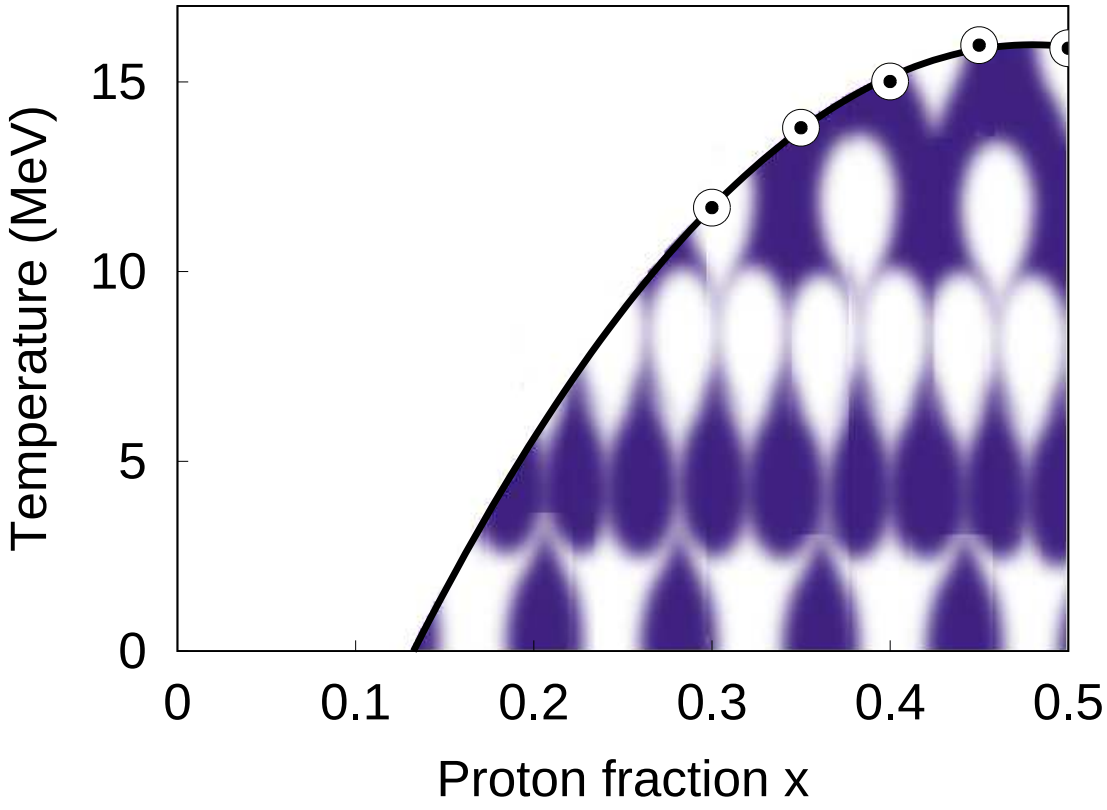

Figure 5.7: Temperature of the critical points as a function of the proton fraction X. The background image under the curve indicates the region where liquid and gas coexist. Extending the trend toward lower values of X, the curve suggest that the lowest X at which liquid and gas can coexist is 0.13.

Chapter 6

Concluding Remarks

6.1 General Conclusion

In the present study we obtained for the first time a phase diagram of infinite nuclear matter which has information in 3-dimension space of $Density\text{-}Temperature\text{-}IsospinAsymmetry$. The liquid-gas coexistence region was obtained by the Maxwell construction method, using volume vs. pressure isotherms obtained through classical molecular dynamics (CMD) simulations and Fermi gas approximations. Such coexistence region is found to be on values of density that went up to $\rho = \rho_0/2$ (with $\rho_0 = 0.16 fm^{-3}$), temperatures of up to $16 MeV$, and isospin content down to $X = 0.13$.

6.2 Future Work

One of the disadvantages of using the CMD code in this thesis is that we did not consider Pauli's exclusion principle, this is because we are not considering quantum phenomena and our study is completely classic.

There is evidence that quantum effects do not allow us to get appropriate results at low temperatures where T is less than $1 MeV$.

Therefore, a path that we can follow as future work is to include such quantum effects on our CMD routine to get more accurate results even at low temperatures. With this we could complement our findings in the low temperature region.

References

[1] B.A. Li, L.W. Chen and C.M. Ko, "Recent Progress and New Challenges in Isospin Physics with Heavy-Ion Reactions", Physics Reports **464** 113 (2008).

[2] C.F.v. Weizsäcker, Zeitschrift fur Physik, **96**, 431-458 (1935).

[3] M.B. Tsang, et al., Phys Rev Lett. **102**, 122701 (2009).

[4] J. A. López, E. Ramírez-Homs, R. González, and R. Ravelo Phys. Rev. **C89**, 024611 (2014).

[5] J.B. Natowitz, G. R opke, S. Typel, D. Blaschke, A. Bonasera, K. Hagel, T. Kl ahn, S. Kowalski, L. Qin, S. Shlomo, R. Wada and H.H. Wolter, PRL **104**, 202501 (2010).

[6] W. Trautmann et al, Int. J. Mod. Phys. **E19**, 1653 (2010).

[7] L.W. Chen, C.M. Ko and B.A. Li, Phys. Rev. **C76**, 054316 (2007).

[8] S. Ulrych and H. Mauther, Phys. Rev. **C56**, 1788 (1997).

[9] E.N.E. van Dalen, C. Fuchs and A. Faessler, Nucl. Phys. **A741**, 227 (2004).

[10] Z.Y. Ma, J. Rong, B.Q. Chen, Z.Y. Zhu and H.Q. Song, Phys. Lett. **B604**, 170 (2004).

[11] F. Sammarruca, W. Barredo and P. Krastev, Phys. Rev. **C71**, 064306 (2005).

[12] E.N.E. van Dalen, C. Fuchs, and A. Faessler, Phys. Rev. Lett. **95**, 022302 (2005).

[13] E.N.E. van Dalen, C. Fuchs, and A. Faessler, Phys. Rev. **C72**, 065803 (2005).

[14] J. Rong, Z.Y. Ma, and N. Van Giai, Phys. Rev. **C73**, 014614 (2006).

[15] I. Bombaci and U. Lombardo, Phys. Rev. **C44**, 1892 (1991).

[16] W. Zuo, L.G. Cao, B.A. Li, U. Lombardo, and C.W. Shen, Phys. Rev. **C72**, 014005 (2005).

[17] V. Baran, M. Colonna, V. Greco, and M. Di Toro, Phys. Rep. **410**, 335 (2005).

[18] C.B. Das, S. Das Gupta, C. Gale, and B.A. Li, Phys. Rev. **C67**, 034611 (2003).

[19] B.A. Li, C. B. Das, S. Das Gupta, and C. Gale, Phys. Rev. **C69**, 011603(R) (2004); Nucl. Phys. **A735**, 563 (2004).

[20] B.A. Li, Phys. Rev. **C69**, 064602 (2004).

[21] L.W. Chen, C.M. Ko, and B.A. Li, Phys. Rev. **C69**, 054606 (2004).

[22] J. Rizzo, M. Colonna, M. Di Toro, and V. Greco, Nucl. Phys. **A732**, 202 (2004).

[23] B. Behera, T.R. Routray, A. Pradhan, S.K. Patra, and P.K. Sahu, Nucl. Phys. **A753**, 367 (2005).

[24] J. Rizzo, M. Colonna, and M. Di Toro, Phys. Rev. **C72**, 064609 (2005).

[25] L. Wilets, E.M. Henley, M. Kraft and A.D. Mackellar, Nuc. Phys. **A282**, 342 (1977)

[26] A. Vicentini, G. Jacucci and V.R. Pandharipande, Phys. Rev. **C31**, 1783 (1985); R. J. Lenk and V. R. Pandharipande, Phys. Rev. **C34**, 177 (1986); R.J. Lenk, T.J. Schlagel and V. R. Pandharipande, Phys. Rev. **C42**,372 (1990).

[27] J.A. López and G. Lübeck, Phys. Lett. **B219**, 215 (1989).

[28] C.O. Dorso and J. Randrup, Phys. Lett. **B301**, 328 (1993).

[29] C.J. Horowitz, M.A. Pérez-García, and J. Piekarewicz, Phys. Rev. **C69**, 045804 (2004).

[30] C.J. Horowitz, M.A. Pérez-García, J. Carriere, D.K. Berry, and J. Piekarewicz, Phys. Rev. **C70**, 065806 (2004).

[31] C.J. Horowitz, M.A. Pérez-García, D.K. Berry, and J. Piekarewicz, Phys. Rev. **C72**, 035801 (2005).

[32] J. Piekarewicz and G. Toledo Sánchez, Phys. Rev. **C85**, 015807 (2012).

[33] C.O. Dorso, P.A. Giménez Molinelli and J.A. López, in "Neutron Star Crust", Eds. C.A. Bertulani and J. Piekarewicz, Nova Science Publishers, ISBN 978-1620819029 (2012).

[34] C.O. Dorso, P.A. Giménez Molinelli and J.A. López, Phys. Rev. **C86**, 055805 (2012).

[35] J.A. López and E Ramírez-Homs, Nuc. Sci. and Tech. **26**, S20502, (2015)

[36] C.O. Dorso, G. Frank, and J.A. López, Nuc. Phys. **A 984**, 77 (2019).

[37] P.A. Giménez Molinelli, J.I. Nichols, J.A. López and C.O. Dorso, Nuc. Phys. **A 923**, 31 (2014).

[38] M.A. Famiano1, T. Liu, W. G. Lynch, M. Mocko, A. M. Rogers, M. B. Tsang, M.S. Wallace, R. J. Charity, S. Komarov, D. G. Sarantites, L.G. Sobotka and G. Verde, Phys. Rev. Lett. **97**, 052701 (2006).

[39] A. Ono, H. Horiuchi, H. Takemoto and R. Wada, Nuc. Phys. **A630**, 148 (1998).

[40] K. Singh Vinayak and S. Kumar, J. Phys. G: Nucl. Part. Phys. **39** 095105 (2012).

[41] S. Kumar and Y.G. Ma, Phys. Rev. **C86**, 051601R (2012).

[42] S. Kumar and Y.G. Ma, Nuc. Phys. **A898**, 57 (2013).

[43] A. Barrañón, C.O. Dorso, J.A. López and J. Morales, Rev. Mex. Fís. **45**, 110 (1999).

[44] A. Chernomoretz, L. Gingras, Y. Larochelle, L. Beaulieu, R. Roy, C. St-Pierre and C. O. Dorso, Phys. Rev. **C65**, 054613 (2002).

[45] A. Barrañón, C.O. Dorso and J.A. López, Rev. Mex. Fís. **47-Sup. 2**, 93 (2001).

[46] A. Barrañón, C.O. Dorso, and J.A. López, Nuclear Phys. **A791**, 222 (2007).

[47] A. Barrañón, R. Cárdenas, C.O. Dorso, and J.A. López, Heavy Ion Phys. **17**, 1, 41 (2003).

[48] C.O. Dorso and J.A. López, Phys. Rev. **C64**, 027602 (2001).

[49] A. Barrañón, J. Escamilla Roa and J.A. López, Braz. J. Phy., **34-3A** 904 (2004).

[50] A. Barrañón, J. Escamilla Roa and J.A. López, Phys. Rev. **C69**, 014601 (2004).

[51] C.O. Dorso, C.R. Escudero, M. Ison and J.A. López, Phys. Rev. **C73**, 044601 (2006).

[52] C.O. Dorso, P.A. Giménez Molinelli and J.A. López, J. Phys. G: Nucl. Part. Phys. **38** 115101 (2011); *ibid*, Rev. Mex. Phys., **S 57 (1)**, 14 (2011).

[53] B.L. Holian, A.F. Voter and R. Ravelo, Phys. Rev. **E52**, 2338 (1995).

[54] H.C. Andersen, J. Chem. Phys. **72** 2384 (1980).

[55] P.J. Siemens, Nature **305**, 29 (1983); *ibid* **336**, 110 (1988)

[56] J.A. López and C. O. Dorso, Lecture Notes on Phase Transitions in Nuclear Matter, World Scientific, ISBN 981-02-4007-4, 2000.

[57] H. Müller, B. Serot, Phys. Rev. **C52**, 2072 (1995).

[58] I. Tanihata, Preprint RIKEN-AF-NP-229, 1996.

[59] W.D. Myers and W.J. Swiatecki, Acta Phys. Pol. **B**26, 111 (1995)

[60] J.A.López, A. Gaytán Terrazas, S. Terrazas Porras, Isospin-dependent phase diagram of nuclear matter, (2019), Nuclear Physics A.

[61] Stanley I. Sandlel, Chemical, Biochemical, and Engineering Thermodynamics, 4th edition, (2005).

Appendix A

Average Energy Tables

Table A.1: Average Energy in MeV for $X = 0.3$

Density ρ (fm^{-3})	T=1	T=2	T=3	T=4	T=5
0.01	−4.759860468	−1.576961532	0.954061266	3.152540963	5.125380573
0.02	−5.059894361	−2.159692462	0.295287184	2.384230072	4.361234427
0.04	−5.187374119	−2.553754959	−0.219165049	1.827495376	3.871541809
0.06	−5.029319496	−2.431157101	−0.124031833	2.005151732	4.041462196
0.08	−4.529336725	−1.896546996	0.444789329	2.619575308	4.791361151
0.10	−3.611289764	−0.948607656	1.505790244	3.775018253	5.955357019
0.12	−2.315846631	0.445109063	2.952618272	5.318289798	7.590024708
0.14	−0.674513986	2.183625549	4.77022218	7.235359005	9.637108072
0.16	1.319224643	4.282388695	6.977545768	9.553361411	11.96203257
0.18	3.632226677	6.702005061	9.515515054	12.11974879	14.60063823
0.20	6.280590413	9.474379042	12.32071684	14.97694919	17.58689166

Table A.2: Average Energy in MeV for $X = 0.3$

Density ρ (fm^{-3})	T=6	T=7	T=8	T=9	T=10
0.01	6.946178674	8.697443114	10.43139716	12.11882593	13.72277229
0.02	6.2176172	8.031987275	9.799398505	11.59320074	13.22458304
0.04	5.75562904	7.678790936	9.443578188	11.25517513	13.08906063
0.06	6.02424391	7.990907955	9.89154045	11.73366771	13.64192381
0.08	6.916295659	8.906940015	10.88962351	12.82082997	14.67828455
0.10	8.101974573	10.21008383	12.1884781	14.32593086	16.15809156
0.12	9.864494878	12.02993079	14.07636899	16.1866821	18.16242937
0.14	11.87127542	14.08348368	16.2721468	18.42938088	20.45877451
0.16	14.27486831	16.62788145	18.84349292	21.03302739	23.15516011
0.18	17.01731176	19.31381941	21.63712995	23.8474606	26.06368593
0.20	20.06698271	22.43226308	24.80874379	27.10521352	29.21114912

Table A.3: Average Energy in MeV for $X = 0.3$

Density ρ (fm^{-3})	T=11	T=12	T=13	T=14	T=15
0.01	15.41972595	16.98127246	18.58266665	20.17580126	21.76030827
0.02	14.94322742	16.56001936	18.26244594	19.92236228	21.46556388
0.04	14.82123691	16.49742509	18.36157282	19.99998021	21.75393718
0.06	15.39002384	17.22320241	19.05439637	20.78656524	22.6965581
0.08	16.53271565	18.59858336	20.32874258	22.22676757	23.99469822
0.10	18.1781732	20.13147056	22.09526515	24.13145061	25.82938171
0.12	20.26367202	22.22998044	24.17832385	26.05804784	28.10625571
0.14	22.54714369	24.61859065	26.68549731	28.68647407	30.69664571
0.16	25.32312774	27.33357964	29.3465943	31.53705195	33.40323499
0.18	28.30547067	30.45156075	32.39371047	34.56602146	36.53876865
0.20	31.43318937	33.66692057	35.83993129	37.92876187	40.11513804

Table A.4: Average Energy in MeV for $X = 0.35$

Density ρ (fm^{-3})	T=1	T=2	T=3	T=4	T=5
0.01	−5.736587979	−2.216812119	0.526044677	2.798737676	4.785712236
0.02	−6.180459064	−2.954118581	−0.42202781	1.756362044	3.734367482
0.04	−6.574327063	−3.739882694	−1.394811731	0.733891455	2.759550848
0.06	−6.82003285	−4.150683512	−1.875331714	0.27204663	2.344636821
0.08	−6.894945638	−4.283548393	−1.954391809	0.268592961	2.373798243
0.10	−6.735101877	−4.066448536	−1.674351308	0.626973319	2.818592815
0.12	−6.273828879	−3.522960359	−0.997062303	1.376420296	3.684626945
0.14	−5.4852681	−2.654043255	−0.010035976	2.485903602	4.775047996
0.16	−4.336754531	−1.370066214	1.348882569	3.856327201	6.313909464
0.18	−2.903095999	0.186379395	2.986951481	5.58268014	8.124243121
0.20	−1.175202157	2.056392956	4.934543355	7.655788888	10.18615885

Table A.5: Average Energy in MeV for $X = 0.35$

Density ρ (fm^{-3})	T=6	T=7	T=8	T=9	T=10
0.01	6.617052965	8.459070839	10.12639374	11.8228686	13.49142953
0.02	5.707568288	7.478900234	9.26974958	10.99871798	12.7063644
0.04	4.665338675	6.520033325	8.389449241	10.20817727	11.97091421
0.06	4.262054558	6.220459729	8.173126322	10.05793363	11.92273383
0.08	4.406144604	6.511541294	8.392840254	10.34908253	12.35701836
0.10	4.962852225	7.073638947	9.044073833	11.09822557	13.11286656
0.12	5.909883712	8.037627114	10.11859553	12.18810181	14.27901851
0.14	7.121282431	9.31094463	11.51451504	13.68518077	15.69744912
0.16	8.627670931	10.96744076	13.19958306	15.29736829	17.48614588
0.18	10.55779184	12.93598073	15.22235816	17.41559725	19.64689895
0.20	12.72219333	15.11093437	17.42557406	19.74972009	22.07130234

Table A.6: Average Energy in MeV for $X = 0.35$

Density ρ (fm^{-3})	T=11	T=12	T=13	T=14	T=15
0.01	15.14477547	16.76576336	18.2420688	19.92624009	21.53962472
0.02	14.41710526	16.02153919	17.73067824	19.34657935	21.0057488
0.04	13.64306718	15.43718311	17.1777423	18.90676832	20.66172604
0.06	13.68098003	15.51841367	17.39983479	19.1895381	20.846914
0.08	14.26300825	15.96089473	17.98537616	19.71539786	21.54236932
0.10	14.99807792	16.99504716	18.94454597	20.76033594	22.66884641
0.12	16.32810836	18.22744383	20.25031395	22.12651847	24.13936416
0.14	17.76949471	19.99124262	21.91023707	23.86253693	25.75529369
0.16	19.72838042	21.78639676	23.76944951	25.91392273	28.06707675
0.18	21.81534712	23.91252762	26.04938622	28.18846312	30.1696579
0.20	24.21015418	26.45148408	28.59104065	30.58707397	32.79892523

Table A.7: Average Energy in MeV for $X = 0.4$

Density ρ (fm^{-3})	T=1	T=2	T=3	T=4	T=5
0.01	−6.595069425	−2.647576959	0.181061811	2.512971987	4.57981014
0.02	−7.1653559	−3.58568612	−0.912250562	1.323291696	3.297822292
0.04	−7.736888118	−4.662565643	−2.235738794	−0.077609058	1.92855562
0.06	−8.169795067	−5.381910941	−3.072889276	−0.936862771	1.126147477
0.08	−8.588074271	−5.990570165	−3.614505879	−1.453244721	0.669721267
0.10	−8.976633367	−6.315205148	−3.912086489	−1.601383491	0.584193878
0.12	−9.118106588	−6.350991069	−3.871805987	−1.51270937	0.823783543
0.14	−8.938153792	−6.063307949	−3.455500075	−0.960827876	1.383194835
0.16	−8.441516375	−5.433215146	−2.726051987	−0.179390352	2.31993201
0.18	−7.648130231	−4.52660314	−1.655756681	0.987193888	3.459345424
0.20	−6.536897324	−3.297443237	−0.357805234	2.35277543	4.887806382

Table A.8: Average Energy in MeV for $X = 0.4$

Density ρ (fm^{-3})	T=6	T=7	T=8	T=9	T=10
0.01	6.386689292	8.246682113	9.940190751	11.6179418	13.2615246
0.02	5.238363577	7.123889171	8.851849512	10.62223102	12.25831906
0.04	3.9688912	5.750234622	7.553018128	9.39277663	11.22026542
0.06	3.092308374	5.025421363	6.975685053	8.697426894	10.71980182
0.08	2.723790562	4.683684699	6.656420255	8.651824783	10.57220467
0.10	2.690452428	4.835129959	6.869056633	8.851892693	10.78117234
0.12	3.11277253	5.160221444	7.339898376	9.388946213	11.48447362
0.14	3.769486093	5.914246805	8.124044647	10.10981053	12.33137727
0.16	4.656234768	6.923963023	9.233109801	11.35751147	13.63877278
0.18	5.935956272	8.285307181	10.53721381	12.76253884	14.94172018
0.20	7.439218251	9.857468362	12.25649314	14.49766707	16.83414016

Table A.9: Average Energy in MeV for $X = 0.4$

Density ρ (fm^{-3})	T=11	T=12	T=13	T=14	T=15
0.01	14.93433813	16.50946013	18.13884459	19.70673739	21.3147825
0.02	13.92927066	15.68378878	17.35812664	18.95240053	20.57458654
0.04	12.92852726	14.70579273	16.44498731	18.12995393	19.79816976
0.06	12.49884179	14.28814946	16.10577855	17.81899136	19.62789387
0.08	12.46168597	14.36527166	16.14256002	18.05582516	19.86002159
0.10	12.79703187	14.75970907	16.64929799	18.50618324	20.37342965
0.12	13.5047876	15.43611326	17.35330817	19.30183029	21.31541923
0.14	14.39321101	16.47437435	18.46991969	20.42115308	22.4780674
0.16	15.66362216	17.82294682	19.77700968	21.88137577	23.95285573
0.18	17.19174379	19.34283903	21.46198316	23.55826272	25.61279635
0.20	19.07115143	21.21540904	23.40701744	25.53359394	27.6324626

Table A.10: Average Energy in MeV for $X = 0.45$

Density ρ (fm^{-3})	T=1	T=2	T=3	T=4	T=5
0.01	−7.268368578	−2.935371861	−0.002924369	2.36812659	4.378432782
0.02	−8.009735499	−3.948421211	−1.235409994	1.018163946	3.072094678
0.04	−8.540773811	−5.186058024	−2.700461261	−0.554254521	1.509723838
0.06	−9.0659595	−6.123219499	−3.817622664	−1.647815692	0.401548806
0.08	−9.634354915	−7.004018587	−4.63055798	−2.405584509	−0.344412389
0.10	−10.30398899	−7.672397083	−5.244717369	−2.977748556	−0.786790891
0.12	−10.82172637	−8.042262884	−5.553118432	−3.172954332	−0.880408119
0.14	−11.02363109	−8.146421459	−5.511364047	−3.071573143	−0.624441947
0.16	−10.91586019	−7.917022415	−5.173386715	−2.576135444	−0.045297937
0.18	−10.49316287	−7.336158211	−4.506381988	−1.842360155	0.694387369
0.20	−9.771390567	−6.487084167	−3.568121168	−0.80774903	1.825601115

Table A.11: Average Energy in MeV for $X = 0.45$

Density ρ (fm^{-3})	T=6	T=7	T=8	T=9	T=10
0.01	6.301141095	8.10149685	9.811066518	11.49802015	13.09861765
0.02	4.950995385	6.786141318	8.632676923	10.40375228	12.15414277
0.04	3.394591156	5.303419422	7.092114047	8.880549607	10.7115786
0.06	2.31616119	4.277551778	6.154925313	8.082785633	9.95842814
0.08	1.675470242	3.742936008	5.732742113	7.612636341	9.575081079
0.10	1.309624251	3.452014805	5.491368332	7.482624839	9.458853846
0.12	1.302361324	3.430245152	5.610960267	7.748458697	9.816984663
0.14	1.656617204	3.862370892	6.075494986	8.180532274	10.19203389
0.16	2.195336061	4.546248232	6.776745364	9.003559522	11.20278175
0.18	3.112239717	5.4940735	7.847449985	10.0404248	12.36672782
0.20	4.303109877	6.735402878	9.137747091	11.35185156	13.58158834

Table A.12: Average Energy in MeV for $X = 0.45$

Density ρ (fm^{-3})	T=11	T=12	T=13	T=14	T=15
0.01	14.81370923	16.4097204	18.03578437	19.59177984	21.16361612
0.02	13.73462941	15.470975	17.15055501	18.75518969	20.36819839
0.04	12.42463314	14.26830251	15.90412227	17.69742728	19.36597925
0.06	11.71377746	13.52352196	15.41613307	17.08576253	18.86605238
0.08	11.35144096	13.3097014	15.10959745	16.94356808	18.72604733
0.10	11.41115057	13.29181442	15.26869159	17.22169803	19.07708479
0.12	11.73874945	13.79922066	15.72038105	17.78573035	19.58441277
0.14	12.37284314	14.37632969	16.49230291	18.40952428	20.44436694
0.16	13.19692052	15.34417035	17.46230603	19.48110163	21.44313339
0.18	14.53758223	16.64212766	18.89052533	20.81838401	22.92050296
0.20	15.99540842	18.07277331	20.31067868	22.45902264	24.54707057

Table A.13: Average Energy in MeV for $X = 0.5$

Density ρ (fm^{-3})	T=1	T=2	T=3	T=4	T=5
0.01	−7.344689647	−3.048605861	−0.090836023	2.268371858	4.408808928
0.02	−8.106402619	−4.098984535	−1.339571106	0.975739423	3.000328359
0.04	−8.758221369	−5.363564212	−2.882291023	−0.693300726	1.320070304
0.06	−9.334598892	−6.389552295	−4.061274146	−1.861306577	0.187662964
0.08	−9.962712093	−7.274124002	−4.965239705	−2.766991273	−0.682136489
0.10	−10.72843597	−8.091468497	−5.680469168	−3.404185279	−1.203583463
0.12	−11.37754907	−8.648557212	−6.106261431	−3.72417737	−1.373076152
0.14	−11.74976111	−8.838000239	−6.202478185	−3.735346833	−1.308000268
0.16	−11.75585937	−8.698166003	−6.01615654	−3.370156719	−0.968206111
0.18	−11.44646798	−8.293511287	−5.43390709	−2.777464164	−0.182440581
0.20	−11.50041451	−7.551790732	−4.625685782	−1.878741804	0.773431256

Table A.14: Average Energy in MeV for $X = 0.5$

Density ρ (fm^{-3})	T=6	T=7	T=8	T=9	T=10
0.01	6.245355459	8.034098445	9.745146238	11.45547218	13.10455001
0.02	4.926739027	6.755033541	8.498671324	10.24131782	11.97912742
0.04	3.193004049	5.1644701	6.965171507	8.795555801	10.4841341
0.06	2.135441299	4.075342614	6.005473207	7.738968649	9.638143743
0.08	1.346005688	3.339779595	5.266844225	7.332509685	9.20140891
0.10	0.934533651	2.969186654	5.044143582	7.053633503	9.012831649
0.12	0.828627362	2.920252301	5.070859122	7.164298311	9.165985891
0.14	0.975559583	3.18375089	5.378747093	7.520835578	9.643573224
0.16	1.409613756	3.76626437	5.960781483	8.158689467	10.32042388
0.18	2.159930169	4.582585715	6.876664413	9.246012058	11.32732958
0.20	3.282477451	5.644887571	8.014805154	10.35875037	12.66780982

Table A.15: Average Energy in MeV for $X = 0.5$

Density ρ (fm^{-3})	T=11	T=12	T=13	T=14	T=15
0.01	14.69463428	16.37542126	18.01561863	19.60364114	21.13214687
0.02	13.68311524	15.30303509	17.03110094	18.59267854	20.28496193
0.04	12.2769125	14.0093278	15.80420068	17.55512872	19.15378877
0.06	11.49441876	13.27949086	15.01425524	16.82624347	18.6453337
0.08	11.06182989	12.93747189	14.76200889	16.58427041	18.42557279
0.10	10.98406227	12.87572523	14.80527236	16.88078915	18.63623949
0.12	11.27016865	13.18043392	15.24026802	17.1961628	19.00145857
0.14	11.73552758	13.72090924	15.75825408	17.84673966	19.76627169
0.16	12.44926674	14.59413063	16.79326176	18.69407827	20.70010737
0.18	13.52923902	15.63396048	17.92144566	19.93862719	22.10574734
0.20	14.83424984	17.09568993	19.26721739	21.21086902	23.54613556

Appendix B

Wolfram Mathematica Routine

To show how the Maxwell construction was performed, we take as example the case of $T = 10MeV$ and $X = 0.5$. The routine was written using the Wolfram Mathematica package. The only thing that is changing between the routines for the different cases are the values of pressure that correspond to the given case, meanwhile, the steps of the routine remain the same.

Temperature T=10 y Proportion X=0.5

In[63]:=
```
dens = {0.04, 0.06, 0.08, 0.10, 0.12, 0.14, 0.16, 0.18, 0.20}
pres = {0.445592, 0.768191, 1.19803, 1.75891, 2.47394, 3.36741, 4.45529, 5.75525, 7.37
mat = {dens, pres} // Transpose
nder = 0.04;
g1 = ListPlot[mat, AxesOrigin → {0, 0}]
fit[n_] = Fit[mat, {1, n, n^2, n^3}, n]
```

Out[63]= {0.04, 0.06, 0.08, 0.1, 0.12, 0.14, 0.16, 0.18, 0.2}

Out[64]= {0.445592, 0.768191, 1.19803, 1.75891, 2.47394, 3.36741, 4.45529, 5.75525, 7.37083}

Out[65]= {{0.04, 0.445592}, {0.06, 0.768191}, {0.08, 1.19803}, {0.1, 1.75891}, {0.12, 2.47394}

Out[67]=

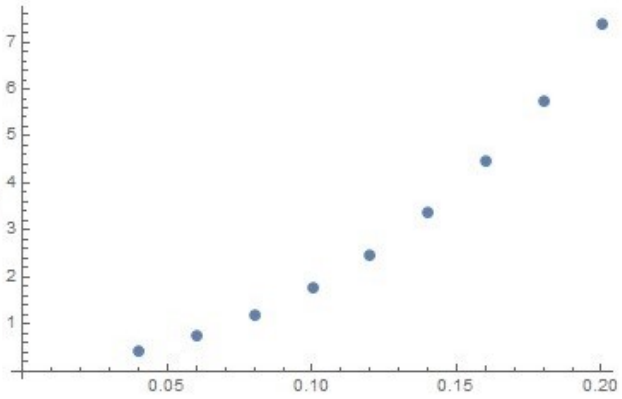

Out[68]= $-0.0264688 + 9.78558\,n + 25.8348\,n^2 + 549.562\,n^3$

Figure B.1: Routine Step 1: We plug the pair of values of pressure vs density for the given case, then we approximate such values using a function of third degree.

In[71]:=
```
Clear[a, T]
ϵ0,1 = 0.693;
ϵ1,1 = -5.420;
ϵ2,1 = 11.447;
ϵ0,2 = 0.037;
ϵ1,2 = 0.082;
ϵ2,2 = -.312;
n0 = 0.15;
ϵT[i_, T_] = Σ_{j=1}^{2} ϵi,j T^j;
ϵT[n_, T_] = Σ_{i=0}^{2} ϵT[i, T] n^i;
a[2] = 21.1;
a[3] = 38.3;
a[4] = 26.7;
a[5] = 35.9;
p[n_, T_] = (n0/3) Σ_{i=2}^{5} i a[i] (n/n0)^(i/3+1) + (2/3) n ϵT[n, T]
```

Out[85]= $0.05\left(996.538\, n^{5/3} + 5106.67\, n^2 + 8933.57\, n^{7/3} + 28258.8\, n^{8/3}\right) + \frac{2}{3}$

In[86]:=
```
pI = Plot[p[n, 10], {n, 0, .02}]
```

Out[86]=

Figure B.2: Routine Step 2: We define the equation of Fermi gas approximation and all its variables, plotted in the low-density region.

```
Clear[d0, d1, d2, d3, sol]
poli[n_] = d0 + d1 * n + d2 * n^2 + d3 * n^3;
dpoli[n_] = D[poli[n], n];
derp[n_] = D[p[n, T], n];
derfit[n_] = D[fit[n], n];
```

In[93]:=

```
nizq = .02; T = 10;
sol = Solve[{poli[nizq] == p[nizq, T],
    dpoli[nizq] == derp[nizq],
    poli[nder] == fit[nder],
    dpoli[nder] == derfit[nder]}]
```

Out[94]= {{d0 → -2.63229, d1 → 312.695, d2 → -10233.7, d3 → 108436.}}

In[95]:=

```
{d0, d1, d2, d3} = {d0, d1, d2, d3} /. sol[[1]]
```

In[96]:=

```
poli[n_] = d0 + d1 * n + d2 * n^2 + d3 * n^3
```

Out[96]= -2.63229 + 312.695 n - 10233.7 n^2 + 108436. n^3

In[97]:=

```
g5 = Plot[poli[n], {n, nizq, nder}, PlotStyle → Red]
```

Out[97]=

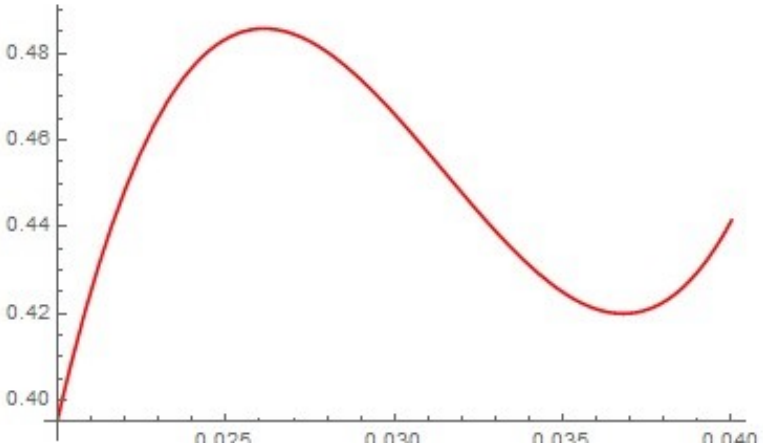

Figure B.3: Routine Step 3: We find the polynomial of third degree that will be used to connect the Fermi gas equation in step 2 and the approximation for the pressure in step 1. This polynomial needs to meet with the conditions of having the same value at the ends, as well as for its first derivative, to make the connection smooth.

In[98]:=

```
Show[pI, g5, g2, AxesOrigin → {0, 0}, PlotRange -> All]
```

Out[98]=

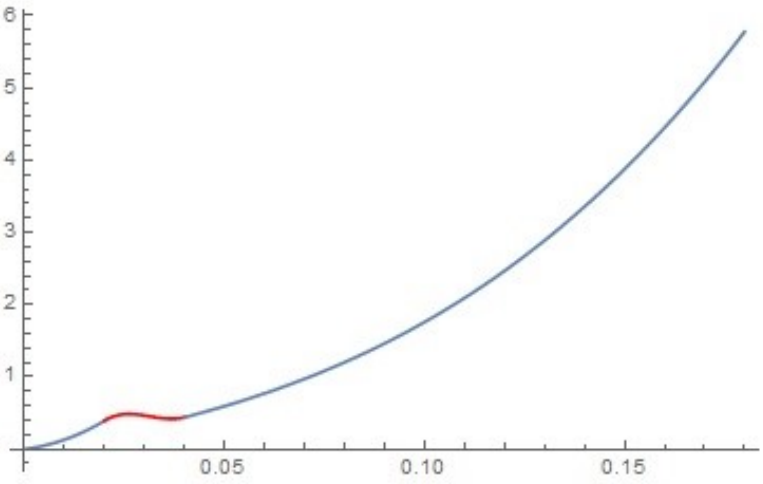

In[100]:=

```
T = 10; nmax = .18;
vmin = 1 / nmax
v1 = 1 / nder
v2 = 1 / nizq
vmax = 1000
pv[v_, T_] = p[n, T] /. n → 1 / v
gas = Plot[pv[v, T], {v, v2, vmax}, AxesOrigin → {0, 0}]
```

Out[101]= 5.55556

Out[102]= 25.

Out[103]= 50.

Out[104]= 1000

Out[105]= $$0.05\left(996.538\left(\frac{1}{v}\right)^{5/3}+8933.57\left(\frac{1}{v}\right)^{7/3}+28258.8\left(\frac{1}{v}\right)^{8/3}+\frac{5106.67}{v^2}\right)$$

Figure B.4: Routine Step 4: We plot all the parts of the curve together and immediately start changing the dependence from density for volume just by substituting $V = 1/\rho$ in each of the expression we already have.

```
dens
vols = 1 / dens // Reverse
```

Out[107]= {0.04, 0.06, 0.08, 0.1, 0.12, 0.14, 0.16, 0.18, 0.2}

Out[108]= {5., 5.55556, 6.25, 7.14286, 8.33333, 10., 12.5, 16.6667, 25.}

In[109]:=
```
mat2 = {vols, pres // Reverse} // Transpose
g1vols = ListPlot[mat2]
```

Out[109]= {{5., 7.37083}, {5.55556, 5.75525}, {6.25, 4.45529}, {7.14286, 3.36741}, {8.33333, 2.47394}, {10., 1.75891}, {12.5, 1.19803}, {16.6667, 0.768191}, {25., 0.445592}}

Out[110]=

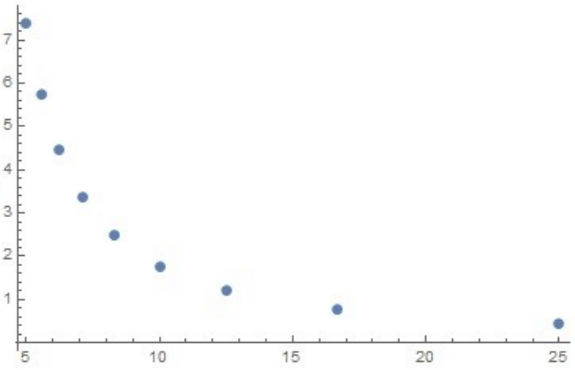

In[111]:=
```
Clear[a, b, c, d]
fit[v_] = NonlinearModelFit[mat2, {d + a / v + b / v^2 + c / v^3}, {a, b, c, d}, v] // Normal
g2vols = Plot[fit[v], {v, vmin, v1}]
Show[g1vols, g2vols, PlotRange → All]
```

Out[112]= $-0.0264688 + \frac{549.562}{v^3} + \frac{25.8348}{v^2} + \frac{9.78558}{v}$

Figure B.5: Routine Step 5: Continue changing the dependence from density for volume just by substituting $V = 1/\rho$ in each of the expression we already have.

```
poli[n_] = d0 + d1 * n + d2 * n^2 + d3 * n^3
poli2[v_] = poli[n] /. n → 1 / v
```

Out[115]= $-2.63229 + 312.695\,n - 10233.7\,n^2 + 108436.\,n^3$

Out[116]= $-2.63229 + \frac{108436.}{v^3} - \frac{10233.7}{v^2} + \frac{312.695}{v}$

In[117]:=

```
g5 = Plot[poli2[v], {v, v1, v2}, PlotStyle → Red, AxesOrigin → {0, 0}]
```

In[118]:=

```
Show[g2vols, g5, PlotRange → All, AxesOrigin → {0, 0}]
```

Out[118]=

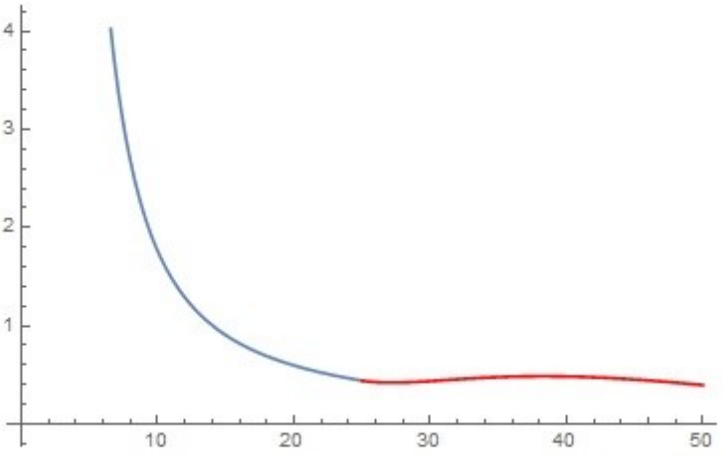

In[119]:=

```
Clear[at, c, area1, area2, area3];
Manipulate[cons = Plot[c, {x, 9, 60}];
 sol1 = FindRoot[fit[v] - c, {v, 9}];
 a = v /. sol1 ; (*este es el extremo izq para la integral*)
 (*ahora hay que integrar de a hasta v1*)
 area1 = NIntegrate[c - fit[v], {v, a, v1}];
 Off[Solve::ratnz];
sol2 = Solve[poli2[v] == c] // Flatten;
```

Figure B.6: Routine Step 6: Once we change the dependence of density to volume, we plot the three parts of the curve together again.

```
b = sol2[[2, 2]];
vf = sol2[[3, 2]];
area2 = NIntegrate[c - poli2[v], {v, v1, b}];
area3 = NIntegrate[c - poli2[v], {v, b, vf}];
area = area1 + area2 + area3;
pf = c;
Show[g2vols, g5, cons, PlotRange → All, AxesOrigin → {0, 0}, PlotLabel → "area = " <> ToString[area]]

, {c, .45, .5, Appearance → "Labeled"}]
```

Out[120]=

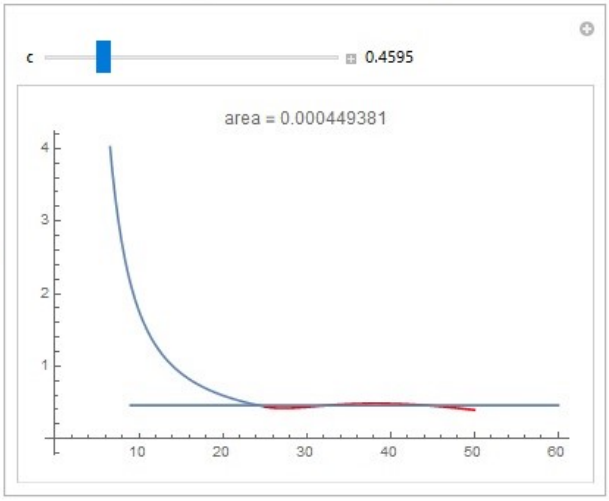

In[121]:=

```
Print[Style["Temperatura = " <> ToString[T], 24, Bold, Blue]]
Print[Style["Presión = " <> ToString[pf], 24, Bold, Blue]]
Print[Style["Volúmenes = " <> ToString[{a, b, vf}], 24, Bold, Blue]]
Print[Style["Densidades = " <> ToString[{1 / a, 1 / b, 1 / vf}], 24, Bold, Blue]]
```

Figure B.7: Routine Step 7: Finally, we designed an interface that find the value of pressure that satisfies the condition that the areas below the curve must be equal, and prints the corresponding values of density and volume where such areas are equal.

Curriculum Vitae

Adrián Gaytán Terrazas was born on August 17th, 1994. He graduated from "Centro de Bachillerato Tecnológico Industrial y de Servicios #114" High School, CD. Juárez, Chihuahua, México in the spring of 2012.

He entered to Universidad Autónoma de Ciudad Juárez on fall of 2012 on the pursuit of his bachelor's degree in Engineering Physics. While pursuing his bachelor's degree he worked as administrative assistant at the Physics and Mathematics department. He received his bachelor's degree on spring of 2017.

In the spring of 2018, he entered the Graduate School of The University of Texas at El Paso. While pursuing a master's degree in Physics he worked as a teaching assistant in the field of physics.

Permanent address: 8128 Jiquilpan.

Juárez, Chihuahua, México 32662